Physics – Uspekhi **60** (9) 911 – 930 (2017)

INSTRUMENTS AND METHODS OF INVESTIGATION PACS numbers: **34.35.+a**, **37.20.+j**, 34.80.Gs

Negative ion adsorption by the ion source surface as a factor influencing ion lifetime measurements

V G Lukin, O G Khvostenko

DOI: https://doi.org/10.3367/UFNe.2017.01.038045

Contents

Abstract. It is well known that negative ions formed in the gas phase through low-energy electron capture by molecules show a scatter in the measured lifetimes of their autodetachment states. In considering this question, it was found that, when using a static sector magnetic mass spectrometer, some of the ions formed on the ionization chamber walls are adsorbed and stabilized there, then joining the registered ion flux and thereby distorting their measured lifetime. Because the number of the adsorbed ions depends on the experimental conditions, their contribution to the total flux is to some extent uncontrollable — hence, the scatter.

Keywords: negative ions, resonance electron capture, mass spectroscopy

1. Introduction

Negative ions play an important role in many physicochemical processes. This accounts for the extensive research into their structure and mechanism of formation and breakdown carried out in recent decades with an emphasis on resonance electron capture (REC) by molecules accompanied by the formation of transient autodetached states of negative molecular ions ($^{a}M^{-}$) [1–9].

Resonance electron capture is an elementary process of interaction between an electron and a molecule that occurs when the molecules of interest are introduced into the gas phase, a high vacuum, to undergo single collisions. The molecules are exposed to a beam of slow monoenergetic electrons with energy E_{el} varying under experimental conditions from 0 to $\sim$ 15 eV, with the result that at certain values of E_{el} the molecules capture an additional electron and give rise to $^{a}M^{-}$ ions. In this way, a series of resonance maxima is formed, each with $^{a}M^{-}$ ions possessing a specific electron configuration depending on which of the existing capture mechanisms operated and which molecular orbitals were involved in the electron attachment. The process proceeds resonantly, because it is realized only at certain E_{el} values and ions thereafter decay along two competing channels: either through autodetachment of the additional electron or due to molecular dissociation into a negative ion (as a rule stable) and a neutral fragment.

A powerful theoretical apparatus has been developed to elucidate the physical nature of autodetachment states of negative $^{a}M^{-}$ ions based on the principles of quantum mechanics [1–21]. Various aspects of the REC process have been considered in the framework of this approach, such as the relationship between discrete and continuous spectra with an estimation of the $^{a}M^{-}$ ion lifetime τ_a relative to autodetachment of the additional electron [11]. The notion of the 'survival factor' was formulated to characterize the competing ion decay channels, i.e., autodetachment and dissociation, and the theoretical expression for electron capture cross section σ by molecules was derived [18]. The measured τ_a

V G Lukin, O G Khvostenko Institute of Molecular and Crystal Physics, Ufa Scientific Center of the Russian Academy of Sciences, prosp. Oktyabrya 71, 450075 Ufa, Russian Federation
E-mail: lukin@anrb.ru

Received 24 May 2016, revised 9 January 2017
Uspekhi Fizicheskikh Nauk **187** (9) 981 – 1002 (2017)
DOI: https://doi.org/10.3367/UFNr.2017.01.038045
Translated by Yu V Morozov; edited by A Radzig

values provided a basis for models taking into account the role of the nuclear subsystem wave function of the molecule–electron system, changes in nuclear configuration during evolution of a negative ion after its formation, and the relative position between electronic terms of the ion and the parent molecule [4, 7, 8]. It was shown that τ_a is related not only to electron capture cross section σ but also to such parameters of the molecule as electron affinity (EA). One of the pioneering articles [19] on resonance electron capture by molecules described the relationship between four characteristics, viz. τ_a, σ, N, and EA, where N is the number of vibrational degrees of freedom in the molecule, and thereby opened up the possibility of estimating EA needed for a variety of applications, from radiation chemistry to electron impact spectroscopy. Reference [4] demonstrated the relationship between EA of the active center and the probability of electron state decay under conditions of electron attachment to a dielectric particle in the gas-discharge plasma.

The lifetime τ_a is one of the principal characteristics of an ion varying over a range from 10^{-15} to 10^{-6} s or wider, within which the $\tau_a \sim 10^{-15} - 10^{-10}$ s region corresponding to short-lived ions lends itself only to theoretical evaluation, whereas the $\tau_a \geqslant 10^{-6}$ s region corresponding to long-lived ions can be estimated both theoretically and in experiment. The value of τ_a is closely related to the shape and mutual position of molecule and ion potential energy surfaces on the energy scale (see Figs 1a–c in review [4]) and to the electron capture mechanism responsible for such an electronic term pattern.

The following are mechanisms of electron capture by a molecule: vibrationally excited Feshbach resonance (VFR) [10], shape resonance (SR) [3], electronically excited Feshbach resonance (EFR) [12], intershell resonance (ISR) [22–24], and a mechanism underlain by intercombination conversion of an 'ordinary' ion doublet ($^2M^-$ with multiplicity $M = 2$) initially formed in one of the EFRs or ISRs [25-30] into an ion quartet $^4M^-$ (with multiplicity $M = 4$). The SR, EFR, and ISR mechanisms correspond to such an arrangement of potential energy surfaces (see Fig. 1a in Ref. [4]) at which the ion potential energy surface lies above the molecular potential energy surface, which accounts for resonance formation for $E_{el} \gg 0$ together with short-lived ions. The VFR mechanism corresponds to the molecular electronic term arrangement shown in Fig. 1b, c [4] at which the process with $E_{el} \sim 0$ is possible and the ions being formed may have $\tau_a \geqslant 10^{-6}$ s. In principle, $^4M^-$ ion quartets can form at any energies E_{el}, including (as a rule) those higher than zero. But even for $E_{el} > 0$, $^4M^-$ ions may have long lifetimes ($\tau_a \geqslant 10^{-6}$ s) commensurate with those of ions in VRF, because of the possible long delay in autodetachment of the additional electron from such an $^4M^-$ ion due to spin prohibition on such autodetachment when the parent molecule has no triplet state with an energy lower than the energy of a given $^4M^-$ ion.

The quantity τ_a is of importance not only in terms of theoretical consideration of the REC process but also from the practical standpoint, since negative ions (NIs) very frequently manifest themselves one way or another in a variety of media, objects, and devices, depending on the ability to confine the additional electron long enough. NIs play an important role in various processes proceeding in the terrestrial ionosphere, giving rise to long-lived negative oxygen molecular ions [4, 31, 32]; they also affect low-temperature plasma dynamics and participate in ion-molecular and biological reactions, including photosynthesis. NIs are exploited in lasers, in modern microelectronic devices and circuits, or to generate accelerator beams. They find application in radiation chemistry, because NIs are known to form in an irradiated material as a result of electron attachment to its molecules [33, 34]. For example, sulfur hexafluoride producing long-lived ions is used as a gaseous insulating material to prevent electric discharges in high-voltage appliances and generators [35]. Recent studies have demonstrated the possible role of spin prohibition in NI quartet states as an effect of occurring the negative differential resistance in microelectronic equipment [30].

Lifetimes τ_a of negative molecular ions $^aM^-$ formed by many compounds has been measured in various laboratories over long periods with the use of various instrumentation techniques, such as time-of-flight mass-spectrometry (TOF MS) [36], static sector magnetic mass-spectrometry (SMS) [37], ion trap mass-spectrometry [38–40], and ion cyclotron resonance (ICR) mass-spectrometry [41–43]. Table 1 presents some of the huge amount of experimental data obtained by different authors in various time periods.

These data illustrate the vast scope of research designed to measure τ_a, as well as problems encountered in experiments, such as the marked discrepancy among results of measurements made by different groups for the same compound, as exemplified by sulfur hexafluoride (SF_6), frequently utilized as a reference specimen for E_{el} scale calibration in REC experiments. The first experimental value of $\tau_a = 10$ μs for SF_6^- was obtained by Edelson and co-workers in 1962 [36]. Thereafter, Stockdale et al. [58] reported $\tau_a(SF_6^-) = 25.8$ μs, Christophorou [59] $\tau_a = 32$ μs, Harland and Thyne [51, 60] $\tau_a = 67$ and 70 μs.

The most striking differences among $\tau_a(SF_6^-)$ values (thousands of microseconds) emerge from ICR and ion trap data [38]. Our measurements made at different periods also yielded τ_a values for SF_6^- ions that varied from 70 to 140 μs.

Such a scatter in the measured lifetimes has been documented for many other compounds; for example, τ_a values of 40 μs [44], 17.5 μs [45], 47.3 μs [46], 48 μs [47], and 90 μs [48] for nitrobenzene ($C_6H_5NO_2^-$) ions have been reported. The authors of the present article obtained τ_a values for these ions in a range from 50 to 90 μs. Another example is hexafluorobenzene, for which the value of 12 μs found in Ref. [49] is significantly different from 35 μs in Ref. [50].

It is worthwhile to mention in this context tetracyano-quino-dimethane (TCNQ), widely applied in modern electronics by virtue of its unusual properties, e.g., a high electrical conductivity of TCNQ–electron donor complexes, comparable to that of metals. A TCNQ molecule exhibits four resonance maxima (at 0, ~ 0.6, ~ 1.4, and 3.2 eV) with long-lived ions, the three latter peaks being associated with the formation of $^4M^-$ ions by means of intercombination conversion [71]. The ion lifetimes τ_a in all four peaks reported by different authors vary by an order of magnitude, namely from 2000–100 μs in Ref. [70] to 33,000–480 μs in Ref. [71]. Even a greater discrepancy (up to three orders of magnitude) was documented for fullerene, another material with high application potential [74, 75], although the measurements were made using similar equipment (a static sector magnetic mass-spectrometer with a magnetic sector analyzer).

A number of hypotheses have been forwarded to explain the scatter in experimental τ_a measurements. The authors of Ref. [44] attributed the difference between $\tau_a(SF_6^-) = 25$ μs obtained by them and 10 μs reported in Ref. [36] to distinct focusing of neutral and charged particles and different

Table 1. Lifetimes τ_a of negative molecular ions of certain compounds with respect to autodetachment of the additional electron; E_{el} is the energy of an electron attached to the molecule.

No.	Compound	Chemical formula	E_{el}, eV	τ_a, 10^{-6} s	References
1	Nitrobenzene	$C_6H_5NO_2$	~ 0	40 17.5 47.3 48 90	[44] [45] [46] [47] [48]
2	Benzonitrile	C_6H_5CN	~ 0	5	[45]
3	Hexafluorobenzene	C_6F_6	~ 0	12 35	[49] [50]
4	Pentafluorobromobenzene	C_6F_5Br	~ 0	21	[45]
5	Pentafluorochlorobenzene	C_6F_5Cl	~ 0	17.6	[45]
6	Pentafluorobenzonitrile	C_6F_5CN	~ 0	17 47	[45] [51]
7	Pentafluorobenzaldehyde	C_6F_5CHO	~ 0	36	[45]
8	Perfluorotoluene	$C_6F_5CF_3$	~ 0	12.2	[52]
9	Tetranitromethane	$C(NO_2)_4$	~ 0	> 1	[52]
10	Glyoxal	$(CHO)_2$	~ 0	2.5	[53]
11	Acetic acid	CH_3COOH	~ 0	326	[54]
12	Malonic acid	$HOOCCH_2COOH$	~ 0	> 1	[54]
13	Adipic acid	$HOOC(CH_2)_4COOH$	~ 0	30	[54]
14	Acrolein	CH_2CHCHO	~ 0	38	[54]
15	Diacetyl	$(CH_3CO)_2$	~ 0	12	[44]
16	Maleimide	$C_4H_2O_2NH$	~ 0	43	[55]
17	Malonic anhydride	$C_4H_2O_3$	~ 0	250	[55]
18	Tetracyanoethylene	$C(CN)_2=C(CN)_2$	~ 0	55 60.7	[56] [54]
19	Phthalic anhydride	$C_8H_4O_3$	~ 0	313	[55]
20	Pyromellitic dianhydride	$C_{10}H_2O_6$	~ 0	8000	[55]
21	Cinnamic aldehyde	$C_6H_5CH=CHCHO$	~ 0	12	[57]
22	Naphthaldehyde	1-$C_{10}H_7CHO$ 2-$C_{10}H_7CHO$	~ 0 ~ 0	16 7.5	[54]
23	Quinoline	C_9H_7N	~ 0	632	[54]
24	Sulphur hexafluoride	SF_6	~ 0	10 25.8 32 70 67 150 10,000	[36] [58] [59] [60] [51] [48] [38]
25	Tris(8-hydroxyquinolinato)aluminum	Alq3	~ 0	800	[61]
26	Pyrene	$C_{16}H_{10}$	~ 0	30	[62]
27	Benzopyrene	$C_{20}H_{12}$	~ 0	40	[62]
28	Anthracene	$C_{14}H_{10}$	~ 0	40 25	[62] [63]
29	Phenanthrene	$C_{14}H_{10}$	~ 0	25	[63]
30	Fluorenone	$C_{13}H_8O$	~ 0	130	[63]
31	2-amino-9-fluorenone	$C_{13}H_9NO$	~ 0	100	[63]

Table 1 (continued).

No.	Compound	Chemical formula	E_{el}, eV	τ_a, 10^{-6} s	References
32	Parabenzoquinone	$O=C_6H_4=O$	2.1 1.35 1.56	30 17 30	[64, 65] [66] [29]
33	1,4-naphthoquinone	$C_{10}H_6O_2$	~ 0 1.5	350 10	[65]
34	Anthraquinone	$C_{14}H_8O_2$	~ 0 0.5 1.8	> 1000 > 1000 18	[63] [63] [63]
35	Duroquinone	$O=C_6(CH_3)_4=O$	1.8	200	[67]
36	Nickelocene	$C_5H_5-Ni-C_5H_5$	~ 0 1.0	100 35	[68]
37	Cobaltocene	$C_5H_5-Co-C_5H_5$	~ 0 1.0	25 15	[68]
38	Pyromellitic acid phenylimide	$C_6H_5-C_{10}N_2O_4H_2-C_6H_5$	~ 0 0.8 1.6 4.2	2200 1500 200 70	[69]
39	Tetracyanoquino-dimethane (TCNQ)	$C_{12}N_4H_4$	~ 0 0.7 1.3 3.2 ~ 0 0.5 1.5 3.2	2000 < 2000 > 100 100 33,000 26,000 49,600 480	[70] [70] [70] [70] [71] [71] [71] [71]
40	Ortho-carborane	$B_{10}H_{10}C_2H_2$	~ 0 0.6	130 45	[72]
41	Azobenzene	C_6H_5-N=N-C_6H_5	~ 0 0.92 1.17	110 25 20	[73]
42	Tetracene	$C_{18}H_{12}$	~ 0 0.6 1.3 2.1 3.1	12,000 5000 1000 120 110	[62]
43	Pentacene	$C_{22}H_{14}$	~ 0 0.4 1.1 1.8	17,000 4500 250 50	[62]
44	Fullerene*	C_{60}	0 – 15 1st maximum 0 eV 2nd maximum ~ 6.5 eV	> 10,000,000 (0) ~ 1,000,000 (6.5)	[74]
			0 – 15 1st maximum 0 eV 2nd maximum ~ 6.5 eV	> 10,000 (0) ~ 1000 (6.5)	[75]

* Energy range (0–15 eV) of ionizing electrons; 1st and 2nd resonance maxima in the effective yield curve at ionizing electron energies of 0 and ~ 6.5 eV, respectively, are presented for fullerene.

conditions in ion sources, such as electron distribution over energies, pressure inside the ionization chamber (IC), and temperature. A similar explanation was proposed by Harland and Thyne [60, 46], who reported a $\tau_a(SF_6^-)$ value almost twice that in Ref. [44]. All the proposed hypotheses were subjected to verification, and most of them proved invalid. Specifically, the authors of study [56] examining the relationship between τ_a and electron energy distribution failed to demonstrate its influence on τ_a. They showed that $\tau_a(SF_6^-) = \text{const}$ within the resonance peak and concluded that electron distribution over energies cannot be a cause of the scatter. The postulated dependence of measured τ_a values on gas pressure inside the IC that could stabilize ions due to collisions with the residual gas was explored by

Odom et al. [42]. Such a possibility was also rejected, since the authors found that only 1% of the ions were involved in collisions at the pressure of 3×10^{-7} mmHg used in their experiment.

One more hypothesis of ion stabilization by exposure to ionizing radiation was proposed in Ref. [76]. However, it too proved untenable, because such an effect possibly occurred only at high pressures. The possible effect of competition between dissociation due to SF_5^- formation from SF_6^- and electron autodetachment was estimated in Ref. [42] applying the ICR technique. This hypothesis also proved to be inconsistent, because the same authors found that 96% of the total ionic current in ICR experiments was composed of SF_6^- ions.

Based on results of a detailed analysis of the putative causes of the scatter in the experimentally measured τ_a values, the majority of authors [38, 77–79] appeared to lean toward the concept of temperature effects with reference to the pioneering work of Klots [80].

According to this concept, $^aM^-$ ions form in an IC in different vibrationally excited states, because initial parent molecules show a thermal distribution over vibrational levels. As a result, transient $^aM^-$ ions with different vibrational energies (therefore different lifetimes) form in the IC. Molecules resided at excited vibrational levels produce shorter-lived ions than molecules occupying the zero vibrational level. Therefore, the ion pool outgoing from the ionization chamber contains ions with different average lifetimes τ_a, and $^aM^-$ ions undergo multiexponential decay. Under these conditions, the measured τ_a becomes a function of both the temperature governing the population of target molecule vibrational levels and the instrumental 'time window' Δt, i.e., of ion flight time in the mass-analyzer tube from the instant of ion formation in the IC to the instant of detection by the first dynode of the secondary emission multiplier (SEM). The higher Δt, the smaller the fraction of short-lived ions that reach the recording system and the higher the measured τ_a value. This suggests a correlation between Δt and τ_a, provided that Δt is varied during the experiment, all other characteristics being unaltered.

It follows from the above that the size of the time window Δt is of importance for the measurement of ion lifetime τ_a with respect to electron autodetachment. The present article focuses on experimental measurements of Δt, its dependence on the various experimental conditions, and the relationship with τ_a, taking into consideration that Δt of the experimental setup being used is the sum of three variables:

$$\Delta t = t_{ext} + t_f + t_{tp} , \quad (1)$$

where t_{ext} is the time of ion extraction from the IC, t_f is the ion time of flight in the mass-spectrometer tube from the IC to the SEM, and t_{tp} is the transient period in the optronic pair (light-emitting diode coupled with a photodiode) of the electronic relay used for measurements. Quantities t_f and t_{tp} in equation (1) are constants (t_f is constant at a fixed accelerating voltage $U_{acc} = 4$ kV); t_f and t_{tp} were measured earlier for the $C_6H_5NO_2^-$ ion at $U_{acc} = 4$ kV and equal to 16.10 ± 0.05 and 20.00 ± 0.05 μs, respectively [50, 81].

Because t_f and t_{tp} are constants, the time window Δt can change, in accordance with formula (1), only with changes in time of ion extraction from the IC. Therefore, we measured t_{ext} with an MI-1201V static sector magnetic mass spectrometer modified for detection of negative ions in the resonant regime to elucidate the relationship between Δt and measured τ_a. Time τ_{ext} being the least known characteristic of the instrument, we measured it together with τ_a under different experimental conditions for the example of sulfur hexafluoride (SF_6), nitrobenzene (NB), duroquinone (DQ), and tetracyanoquino-dimethane (TCNQ). Some analogous data for SF_6 and DQ molecules were obtained earlier by the authors of Refs [82, 83], who postulated one more cause of the scatter in the SMS-measured τ_a values, besides well known temperature multiexponentiality, namely ion adsorption on the IC walls. The present work was designed to gain a deeper insight into this phenomenon by increasing the number of study subjects and extending the variety of experimental conditions.

2. Experimental setup

Studies were carried out using a commercially-produced MI-1201V SMS [84, 85] modernized for detection of negative ions in the resonant mode of slow ($E_{el} = 0-15$ eV) electron capture by molecules [86] and equipped with an oscillograph for t_f and Δt measurements [50, 81] (see Fig. 1). Instruments in this series are sector magnetic mass spectrometers with an analyzer tube bend angle of 90° initially intended for discrete analysis of the isotope composition of gases and solids. To adapt the instrument for operation with negative ions produced via REC, lenses of the electron-optical system of the ion gas source in MI-1201V [87] were readjusted without altering the ion-optical system of the ion source. The functional assemblies of the instrument were connected reversibly. The modernized electron-optical system of the ion source made it possible to individually regulate lens potentials and thereby focus on the collector an electron beam with energy $E_{el} = 0-15$ eV and distribution half-width $E_{1/2} \approx 0.3-0.5$ eV.

An SEM was employed to improve sensitivity of NI recording because NI formation cross section is several orders of magnitude smaller than that of positive ions. The first dynode of the 17-cascade multiplier coupled to the high-ohmic input of the electrometer amplifier was grounded, and its collector, the electrometer itself, and the cable connecting it to a direct-current amplifier (DCA) are held at the SEM supply voltage. This SEM connection circuit is not quite secure and requires double screening of the units held at supply voltage to avoid interference, which it implies the use of an interface device coupling DCA with recording instruments. However, it is such an arrangement that is best suited for the measurement of NI lifetimes, since it makes the detector equally sensitive to neutral and charged particles resulting from autodetachment of the additional electron, as particles with the same energy, which needs to be taken into consideration in ion lifetime measurements. The SEM can be connected not only to a DCA but also to a broad-band pulse amplifier through a blocking capacitor (see Fig. 1).

The mass spectrometer was connected to an IBM personal computer in compliance with the Computer-Aided Measurement And Control (CAMAC) standard via the APEK 5.0 interface unit (provided by Research and Engineering Center of Russian Academy of Sciences, Chernogolovka, Moscow region) [88]. The software is written in the Visual Basic language. The substance of interest is introduced into the IC either directly or through a 'comb' [89]. Electrons emitted by the W-cathode interact with substance vapors and give rise to negative ions that arrive at the outlet end of the ionization

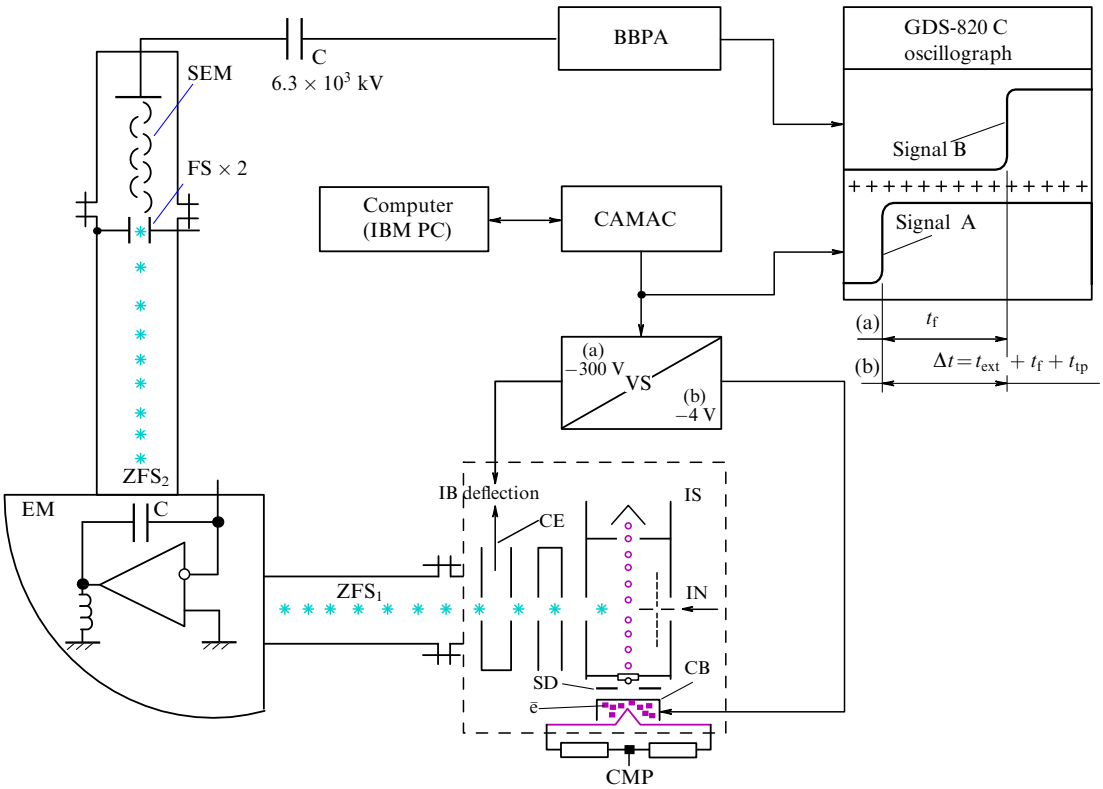

Figure 1. Block diagram of a modernized MI-1201V mass spectrometer coupled to GDS-820C two-channel digital oscillograph: VS — voltage source, IS — ion source, IN — inlet channel, CB — cathode box, SD — shielding diaphragm of the ion source (nicknamed fox), CE — correcting electrode, CMP — cathode midpoint, IB — ion beam, ZFS — zero-field space, EM — electromagnet, SEM — secondary emission multiplier, C — capacitor, and BBPA — broadband pulse amplifier.

chamber under the influence of the electrostatic field of the repel electrode and find themselves in the field of the extractor electrode placed behind the exit slit with applied positive potential U_{ext}. Ions are extracted from the IC under the effect of the potential U_{ext}, then accelerated, separated according to their mass numbers (m/z), and recorded.

Online research is a two-step procedure, because a mass spectrum of resonance electron capture by molecules exhibits a 3D array of effective yield curves (EYCs): *mass number–intensity–electron energy*. First, the NI mass spectrum is recorded in a given mass number range with simultaneous scanning of electron energy from 0 to 15 eV; thereafter ion EYCs are plotted for each m/z value.

SMA studies were carried out with the following adjustment parameters of the ion source: electron energy distribution width $E_{el} \approx 0.3-0.4$ eV at the EYC half-height for SF_6^- ions, electron current of ≈ 1 μA, and accelerating voltage of 4 kV. Electron energy scale linearity was calibrated against SF_6^- ion EYC maxima (zero energy) from SF_6 and $C_6H_5^-$ (8.0 eV) from C_6H_6.

3. Method for the measurement of negative ion lifetime and time of ion extraction from the ionization chamber

The method utilized for measurements of negative ion mean lifetime τ_a with respect to electron autodetachment is based on the separation of neutral component N^0 from the total N beam with subsequent recording of EYCs for particles of both types [47, 90]. The neutral component N^0 is represented by M^0 molecules formed from NIs that lost the additional electron. N^0 is separated in the electric field of a flat capacitor placed in front of an SEM by applying a negative potential of 1–1.5 kV to its plates. Under these conditions, ions deflect from the beam, and it contains only the neutral component N^0. Autodetachment of the additional electron from a negative ion shows statistical behavior like that of radioactive decay. Accordingly, some of the ions undergo autodetachment of the additional electron for the time of flight t from the mass analyzer to the first SEM dynode (electric and magnetic field-free space — the second zero-field region in Fig. 1) and turn into neutral molecules, so that

$$N^- = N \exp\left(-\frac{t}{\tau_a}\right), \tag{2}$$

where N^- is the number of ions retained for time t, N is the 'initial' number of ions entering into the second zero-field region at instant $t = 0$, and τ_a is the mean NI lifetime. Notice that $N = N^- + N^0$, where N^0 is the number of ions broken down for time t (see above). Clearly, it follows from this equation that $N^- = N - N^0$. Substituting the last equality into expression (2) yields $N - N^0 = N \exp(-t/\tau_a)$, whence the formula for calculating τ_a:

$$\tau_a = \frac{t}{\ln\left[(N - N^0)/N\right]}. \tag{3}$$

In expression (3), both quantities needed are measurable: N stands for the ion pool entering to the straight segment of the second zero-field region, the general signal reaching the recording system within this segment. It contains both ions that have failed to decay on the straight segment and neutral

particles originating from the decay of part of the ions. However, the overall intensity of the signal coming up to the recording system is exactly equivalent to the initial number of ions entering the straight segment. At the same time, the number of ions broken down on this segment (N^0) is recorded as a signal remaining after removal of the ion component from the total flux by deflecting plates.

The method of t_f measurement implemented in the present study is similar to that for Δt measurement: in both cases, a two-channel GDS-820C oscillograph is used [91], the only difference being that as t_f is measured, the ion beam is blocked/unblocked by applying/removing a $\sim$ 300-V negative potential to/from the correcting electrode (CE) (see Fig. 1), whereas Δt is determined with a blocking/unblocking of the electron beam by applying $\approx$ 4-V negative potential to the modulator, i.e., the cathode box (CB) (see Fig. 1), to block/unblock electron current entering the IC. The Δt measurement procedure is controlled by an electronic relay [81], because the electron-optical system of the ion source is under NI-accelerating potential. In both methods, the oscilloscope is exploited in the regime of a single sweep triggering with synchronization along the signal's leading edge, when the sweep can be triggered only in the presence of a triggering (input) signal, the amplitude of which has to exceed the sweep-triggering level. The sweep-triggering signal is fed into one of the GDS-820C channels via CAMAC from the IBM personal computer to synchronously trigger the sweeps of both channels, with the result displayed on the oscilloscope screen. The signal from the broadband pulse amplifier connected to the SEM through the blocking capacitor (see Fig. 1) is fed into the second channel to be recorded by the oscillograph as the arrival of the NI beam at the first dynode. The difference between the two signals gives either t_f or Δt, depending on the procedure employed. After both t_f and Δt are measured, it is possible to evaluate $t_{ext} = \Delta t - (t_f + t_{tp})$.

4. Results of the measurement of negative ion lifetime and time of ion extraction from the ionization chamber

All SF_6 and NB experiments described below were conducted for a peak of molecular negative ions formed at $E_{el} \sim 0$ by the VFR mechanism [59]. The peak at $E_{el} \sim 1.8$ eV corresponding to $^4M^-$ ion quartets was utilized in the case of DQ [67], while the maximally intense peak at an energy of 0.5 eV, also represented by $^4M^-$ ions, was involved in TCNQ experiments [71].

The values of t_{ext} and τ_a, as well as intensities (Int) of molecular negative ions, were measured as functions of inflows of different amounts of SF_6, NB, and DQ into the IC (Fig. 2). Figure 3 plots EYCs of negative SF_6 ions and the neutral component, providing the basis for τ_a measurements using formula (3), and the dependence of ion lifetime τ_a on electron energy. The data depicted in Fig. 3a were obtained for an inflow of a minimal amount of the substance to be analyzed into the IC, when the rotation number of the gas puffing valve was $n_c = 1$ (Fig. 2a) and those of Fig. 3b for a maximum inflow ($n_c = 7$, Fig. 2a). It follows from Fig. 3 that a change in the relative content of ionic and neutral components of the signal with a growing amount of the substance allowed in to the IC results in a decrease in τ_a from 94 to 89.6 μs. Figure 2 also shows that the inflow of increased amounts of all three substances (SF_6, NB, and DQ)

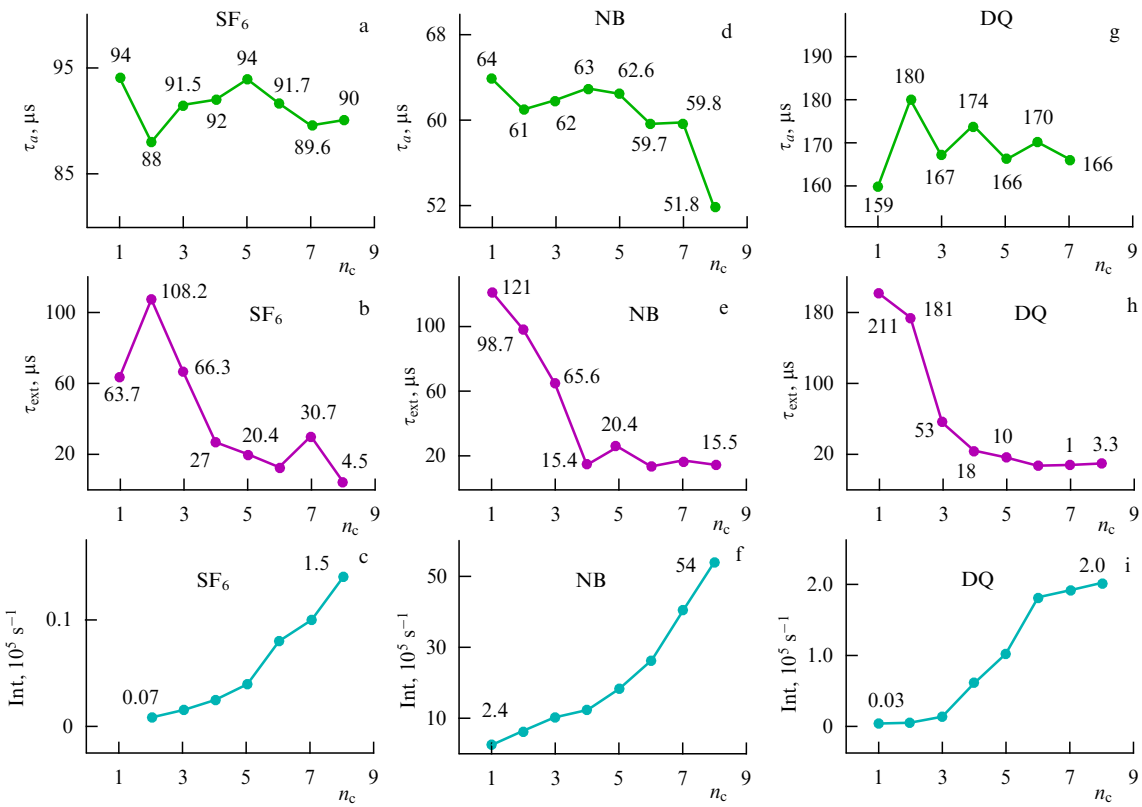

Figure 2. Lifetime τ_a, time t_{ext} of ion extraction from ionization chamber, and intensity (Int) of molecular negative ions for SF_6 (a–c), NB (d–f), and DQ (g–i), respectively, depending on the amount of substance introduced into the ionization chamber; n_c is the rotation number of a gas puffing valve.

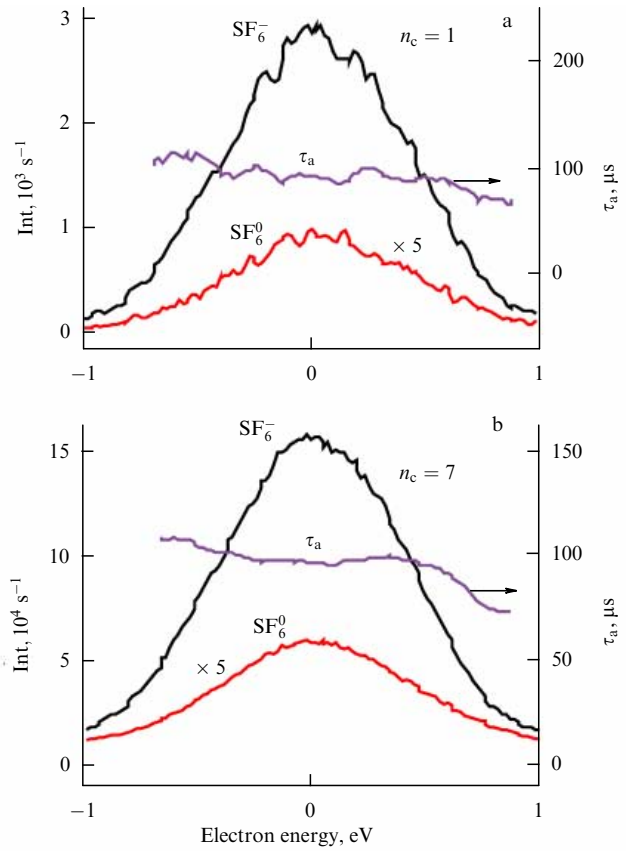

Figure 3. Effective yield curves for negative SF_6^- ions and neutral SF_6^0 molecules (ion decay products) and plots of ion lifetime τ_a vs electron energy for small (a) and maximum (b) SF_6 gas puffing into an IC.

is associated with the consistent enhancement of ion intensity and the reduction in t_{ext}. The character of τ_a changes is not uniform, being specific for each compound. In SF_6 and DQ, lifetime τ_a oscillates chaotically with growing inflow, whereas it tends to steadily decrease in NB.

Dependences of t_{ext}, τ_a, and Int on IC temperature T^0 were found for SF_6, NB, DQ (Fig. 4), and TCNQ (Fig. 5). Baseline EYCs for NB ions and neutral components are presented in Fig. 6 together with the respective plot of τ_a vs electron energy at a temperature rise in IC from 60 to 200 °C. Figure 4 demonstrates that, in the case of SF_6, NB, and DQ, a rise in T^0 leads to a uniform increase in t_{ext} with a simultaneous decrease in τ_a and Int. The decrease in τ_a is quite apparent in the curves for the ion and neutral components in Fig. 6 from the latter's enhanced relative intensity responsible for reducing the NB lifetime from 66.3 μs at 60 °C to 31.8 μs at 200 °C. Thus, there is a strongly pronounced tendency toward reverse correlation between t_{ext} and τ_a on which a weak linear dependence among them is superimposed. This weak dependence is analogous to the upper harmonic of a radiowave signal superimposed on a lower frequency. In the case of t_{ext} and τ_a, the direct dependence between two 'high-frequency' characteristics corresponds to synchronous changes in both variables. The case of TCNQ is altogether different from that of the three other compounds (see Fig. 5) for which t_{ext}, τ_a, and Int vary chaotically as temperature rises.

For SF_6, NB, DQ, and TCNQ molecules, quantities t_{ext}, τ_a, and Int were measured as functions of helium inflow to the ionization chamber (Figs 7 and 8). Effective yield curves for ions and neutral molecules, together with the corresponding

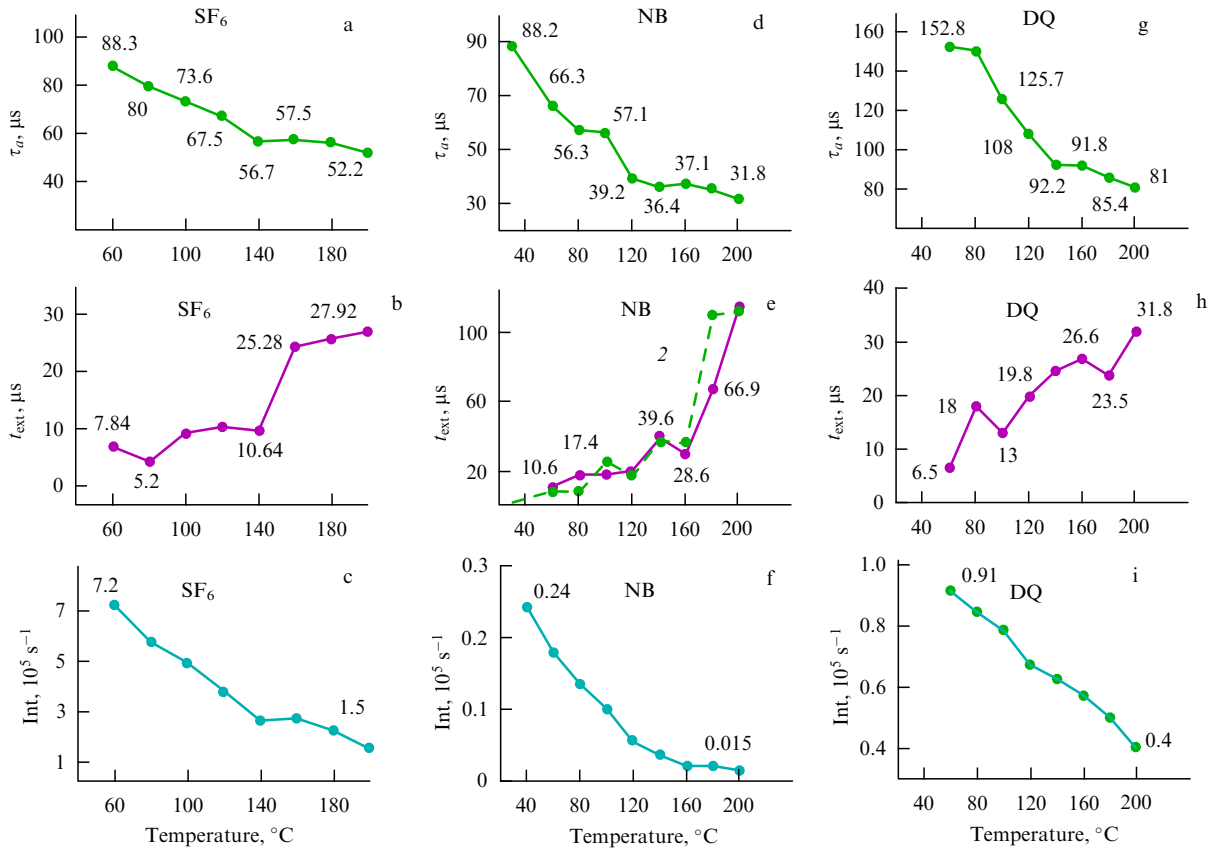

Figure 4. Lifetime τ_a, time t_{ext} of ion extraction from ionization chamber, and intensity (Int) of SF_6 (a–c), NB (d–f), and DQ (g–i) molecular negative ions, respectively, plotted vs IC temperature. Curves *1* and *2* in figure (e) show measurements after a given temperature was reached and 15 min later, respectively.

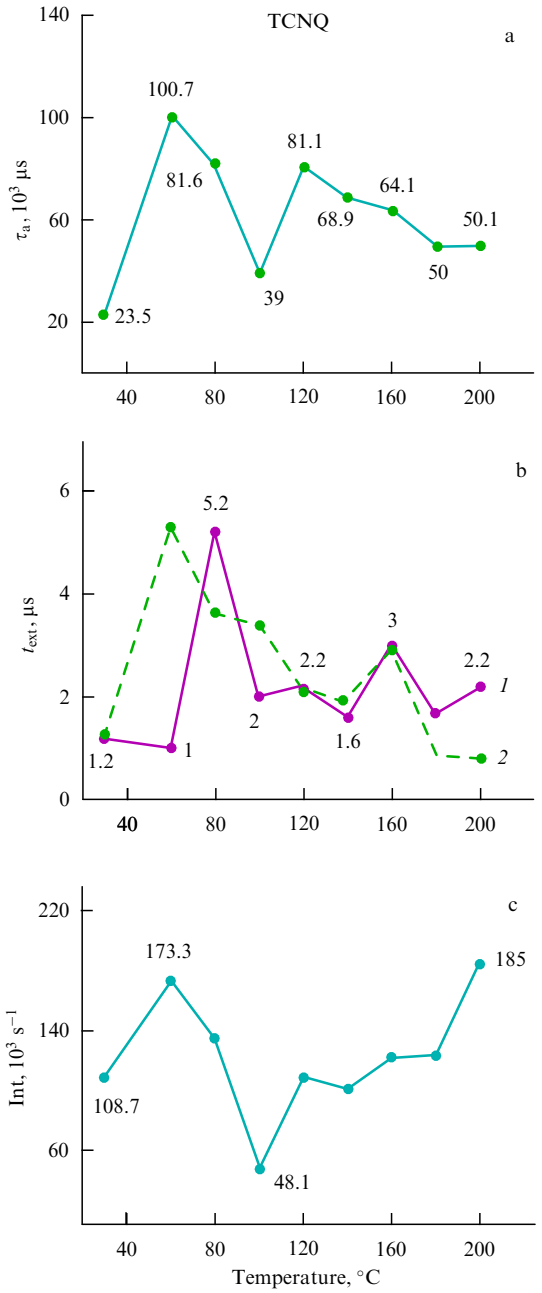

Figure 5. Lifetime (a), time of ion extraction from ionization chamber (b), and intensity (c) of negative TCNQ ions depending on IC temperature. Curves *1* and *2* in figure (b) show measurements after a given temperature was reached and 15 min later, respectively.

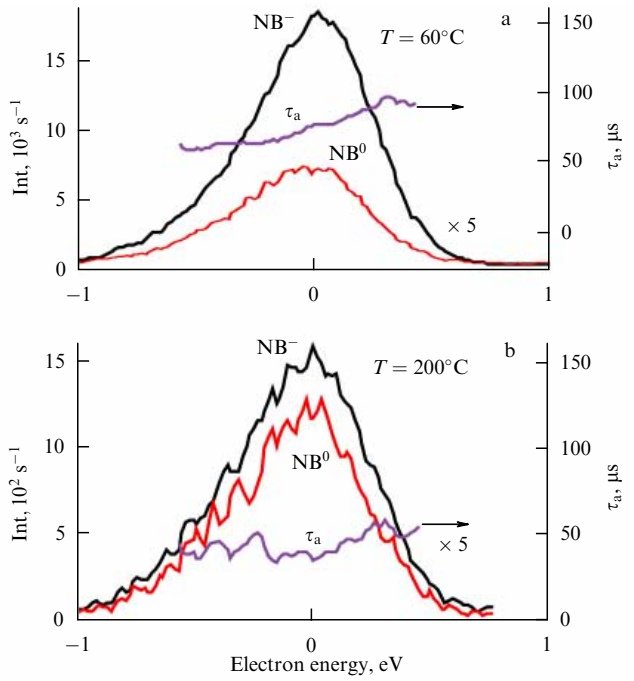

Figure 6. Effective yield curves for NB^- ions and neutral NB^0 molecules (ion decay products) and plots of ion lifetime τ_a vs electron energy at IC temperature $T = 60$ °C (a) and $T = 200$ °C (b).

τ_a plot for TCNQ at small and maximum helium inflows, are presented in Fig. 9, demonstrating the strong influence of the helium inflow on τ_a, which decreases by two orders of magnitude (from 50,000 to 500 μs at the intensity maximum at 0.5 eV) as the number of helium puffing valve rotations increases from $n_{He} = 1$ to $n_{He} = 7$. It is worthy of noting that changes in t_{ext} and τ_a in the case of SF_6 with an increasing amount of helium inflow into the IC (see Fig. 7) are largely similar to those associated with a rise in T^0, i.e., t_{ext} increases and τ_a decreases, while intensity remains unaltered. The case of NB (see Fig. 7) is characterized by a manifestation of the three-step dynamics of measured parameters corresponding to those of helium inflow, viz. a rise from $n_{He} = 1$ to $n_{He} = 5$ is associated with decreasing t_{ext} and increasing τ_a, and especially Int; a rise from $n_{He} = 5$ to $n_{He} = 7$ leads to a synchronous increase in t_{ext} and τ_a with practically unaltered Int, and, finally, a rise from $n_{He} = 7$ to $n_{He} = 8$ results in a similar synchronous increase in t_{ext} and τ_a, but a sharp decrease in Int. The duroquinone (DQ) ions (see Fig. 8) exhibited a weak increase in t_{ext} and a sharp decrease in both τ_a and Int. The behavior of TCNQ ions (see Fig. 8) was similar to that observed at elevated temperatures, when t_{ext} increases, while τ_a and Int decrease.

Dependences of t_{ext}, τ_a, and Int on extractor voltage U_{ext} were also studied for SF_6, NB, DQ, and TCNQ (Figs 10–13). Figure 14 illustrates the electron energy dependences of τ_a and corresponding EYCs for ions and neutral particles of DQ, when there is a change in U_{ext} from 30 to 40 V. It follows from Figs 10–14 that a rise in U_{ext} always causes an increase in Int and a decrease in the whole of t_{ext}. At the same time, changes in τ_a are different for individual compounds, as in some other experiments. In the cases of SF_6 (Fig. 10a–c and d–f) and NB (Fig. 11a–c and d–f), a rise in U_{ext} causes τ_a to decrease. These four measurements demonstrate a direct correlation between t_{ext} and τ_a as both diminish. However, other measurements for SF_6 (Fig. 10g–i) and NB (Fig. 11g–i) showed an increase in τ_a with increasing U_{ext}. In the cases of DQ and TCNQ, τ_a either oscillates as U_{ext} increases, which accounts for a 'certain noisiness' of the plots (Figs 12a and 13a) or remains unaltered (Fig. 13d, g). In the case of DQ, the degrees of noisiness are virtually identical for t_{ext} and τ_a (Fig. 12a, b) by virtue of the direct relationship between them, analogous to the aforementioned 'upper' harmonic, the only difference being that this direct dependence is not weak. A change in τ_a with increasing U_{ext} in the case of TCNQ ions (Fig. 13d, g) is impossible to characterize because of its extremely high value, indicative of an infinitely long lifetime.

Dependences of t_{ext} and τ_a on lens potentials of the ion source were studied for SF_6 and DQ molecular ions. The potentials were changed at the repel electrode (U_r) (see Fig. 15) and the first fox (U_F) (see Fig. 16). An increase in

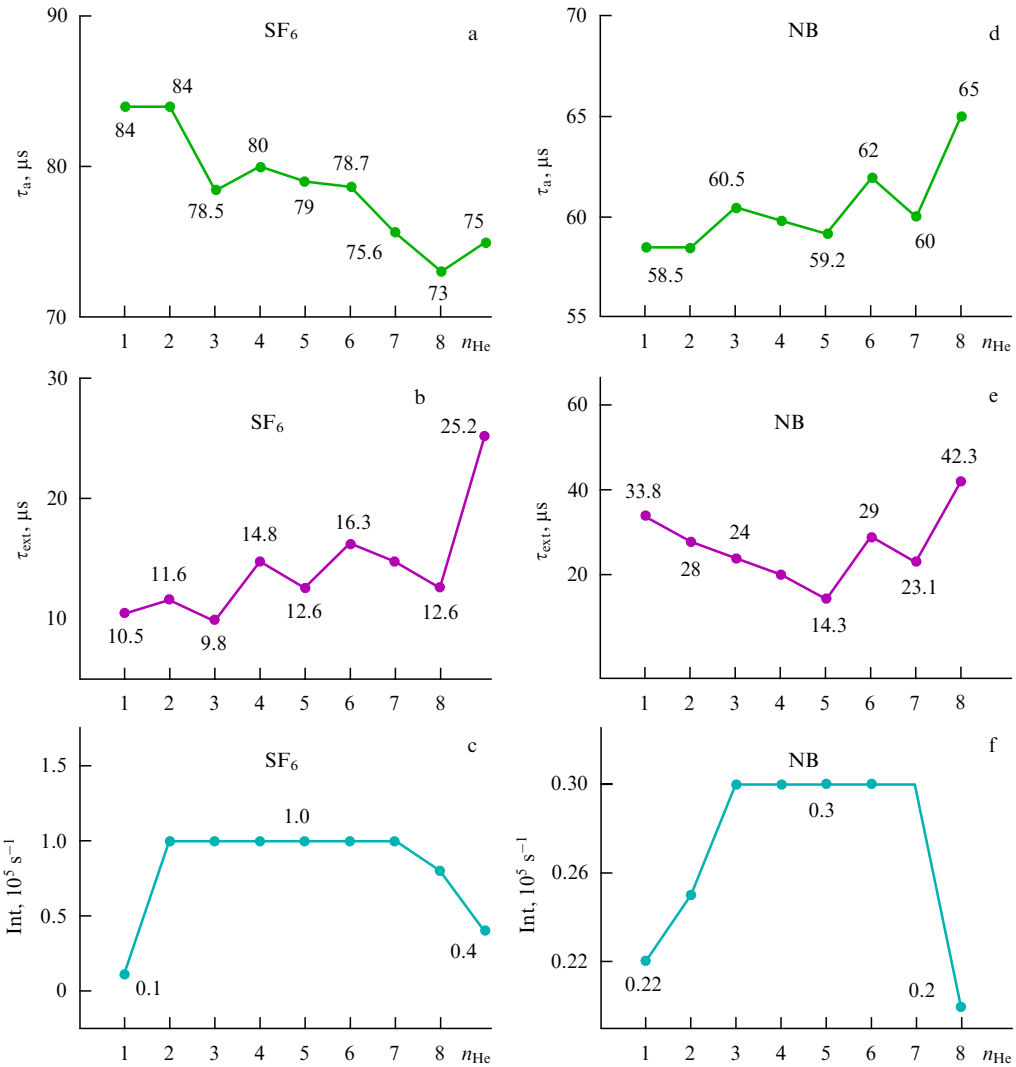

Figure 7. Lifetime τ_a, time t_{ext} of ion extraction from ionization chamber, and intensity, respectively, of SF_6 (a–c) and NB (d–f) molecular negative ions plotted vs the amount of helium bleed-in to the IC; n_{He} is the rotation number of helium puffing valve.

both potentials U_r and U_F caused an extension of t_{ext} and τ_a for all substances but DQ, in which a rise in U_r was accompanied by a decrease in t_{ext} over the entire range; it increased only at the last point (see Fig. 15). The curves demonstrating a general increase in t_{ext} and τ_a were sometimes superimposed by the aforementioned 'higher harmonic', with the inverse relationship between t_{ext} and τ_a in both measurements for the case of SF_6 (Fig. 15a, b and Fig. 16d, e) and rather with the direct relationship in the case of DQ (Fig. 16d, e). In addition, a variation in U_r in DQ (see Fig. 15) and U_F in SF_6 (see Fig. 16) measurements revealed the direct dependence between τ_a and Int. In the course of U_r variations in SF_6, maximum SF_6 and DQ ion intensities were observed at $U_r = -2$ V (Fig. 15c) and $U_r = -0.5$ V (Fig. 15f), respectively.

5. Discussion of measurement results

5.1 Absence of correlation between time window and measured lifetime

It follows from the data available that τ_a and t_{ext} measured in the present work for SF_6^-, DQ^-, NB^-, and $TCNQ^-$ ions with the aid of an MI-1201V SMS at different times show a marked scatter even under the standard experimental conditions with nominal lens potentials of the ion source (Table 2). For example, the scatter of τ_a values for SF_6^- and DQ was $78-106 = 28$ and $150-190 = 40$ μs, respectively. Comparing these values with the data in Table 1 for the same compounds shows that they are commensurate with the discrepancies between τ_a measurements reported in the literature.

Times of ion extraction from the IC, presented in Table 2, differ as well, with the range of t_{ext} scatter being wider than that of τ_a. A characteristic example is t_{ext} (DQ^-), varying from 6.5 to 1020 μs. Notice that no correlation between τ_a and t_{ext} for any compound has been documented in different measurements. Such a scatter in τ_a and t_{ext} values and the absence of correlation between them cannot be accounted for in terms of the aforementioned temperature multiexponentiality concept alone, because IC temperature in the experiments being described remained constant ($T \pm 0.5$ K). This suggests the involvement of one more factor having influence on τ_a measurements. The nature of this effect can be deduced from t_{ext} values.

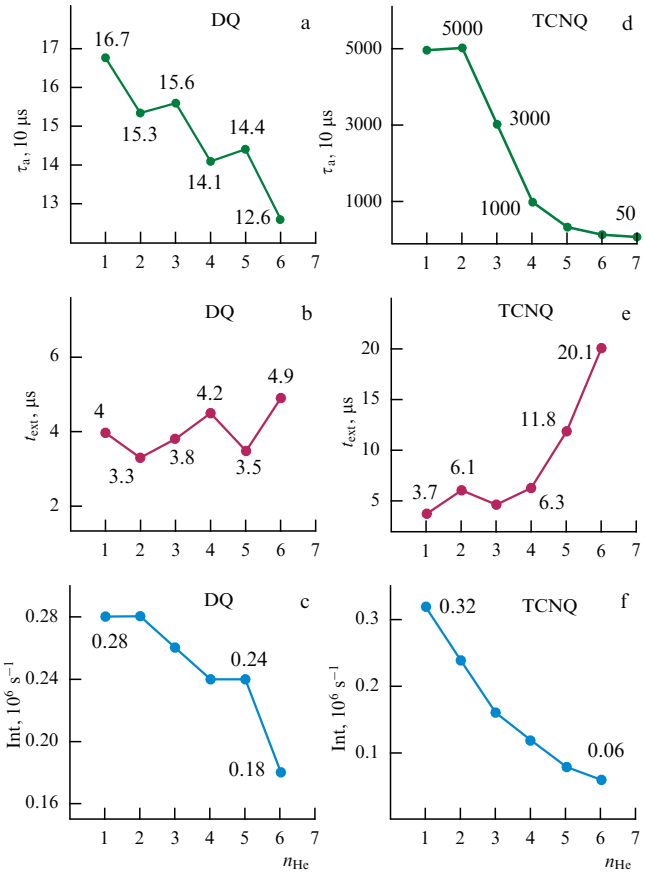

Figure 8. Lifetime τ_a, time t_{ext} of ion extraction from ionization chamber, and intensity of DQ (a–c) and TCNQ (d–f) molecular negative ions depending on the amount of helium bleed-in to the IC.

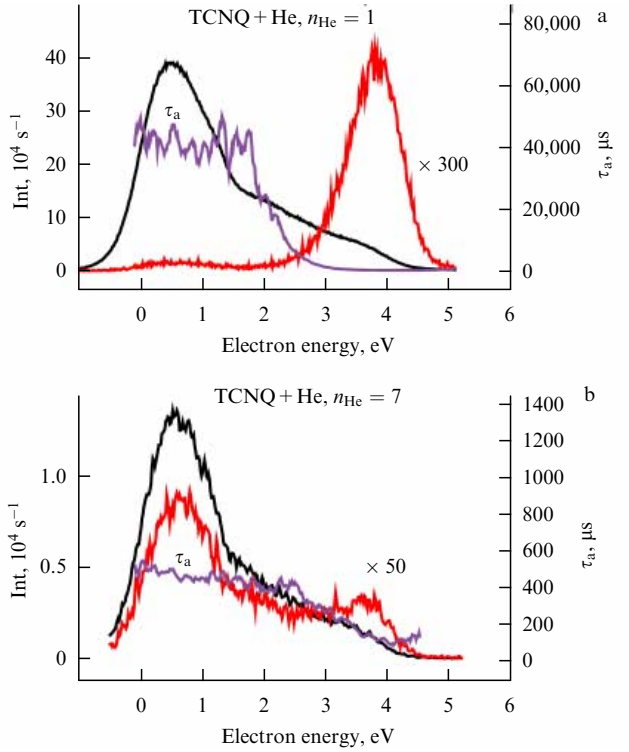

Figure 9. (Color online.) EYCs for TCNQ ions (black curve) and neutral $TCNQ^0$ molecules (ion decay products) (red curve) and dependence of ion lifetime τ_a on electron energy for small (a) and maximum (b) He inflow into the IC.

5.2 Time of ion extraction from the ionization chamber

Many but not all t_{ext} values obtained in the present study significantly exceed the evaluated time t_{calc} of free $^aM^-$ ion escape from the chamber (see Table 2). The values of t_{calc} presented in Table 2 were calculated for all compounds of interest at a nominal repel electrode voltage of ~ 1 V as practiced in MI-1201V SMS experiments with the use of the expression [92]

$$t_{calc} = 1.44 \times 10^{-6} \sqrt{\frac{M_i}{ZU_r}}\, d, \qquad (4)$$

where t_{calc} is the estimated time of free $^aM^-$ ion escape from the chamber in seconds, M_i is the ion molecular weight, Z is the ion-to-electron charge ratio, U_r is the repel electrode potential in volts, and $d \approx 0.5$ cm is the ion flight path between the ionization region and the chamber cover. It follows from Table 2 that t_{calc} for SF_6^- reaches 6.0 μs, whereas its t_{ext} was 11.8 μs in one of the measurements. A marked discrepancy was documented for DQ negative ions: t_{calc} $(DQ^-) = 6.4$ μs and $t_{ext} = 1020$ μs, etc.

Similar results were obtained in Refs [82, 83], which enabled the authors to conclude that ion retention in the IC is due to their adsorption on the walls. To recall, the effect of NI surface adsorption in the experimental setup was also reported by other authors [93], who had to take special

Table 2. Lifetime τ_a and time t_{ext} of SF_6^-, DQ^-, NB^-, and $TCNQ^-$ ion extraction from IC, measured with an MI-1201V SMS depending on measurement date; t_{calc} is the estimated time of free ion escape from the ionization chamber.

Experimental values τ_a and t_{ext}, μs									Scatter of τ_a and t_{ext} values, μs	t_{calc}, μs
SF_6^-	τ_a	88.3	80.1	79.6	106	92.2	78.7	89.5	78–106	—
	t_{ext}	7.87	8.44	8.48	9.6	9.84	10.56	11.8	8–12	6.0
DQ^-	τ_a	191	152.8	166	165	179.3	177.6	159	150–190	—
	t_{ext}	11.8	6.5	1020	64.5	33.5	180	211	6–1020	6.4
NB^-	τ_a	54.7	59	51.8	66.3	50	62.4	63.7	50–66	—
	t_{ext}	15.2	27.3	15.5	10.6	22.8	10.7	8.9	9–23	5.5
$TCNQ^-$	τ_a	6×10^4	5×10^4	4.6×10^4	2.3×10^4	—	—	—	$2 \times 10^4 - 6 \times 10^4$	—
	t_{ext}	41.9	42.7	9.6	1.2	—	—	—	1–42	7.1

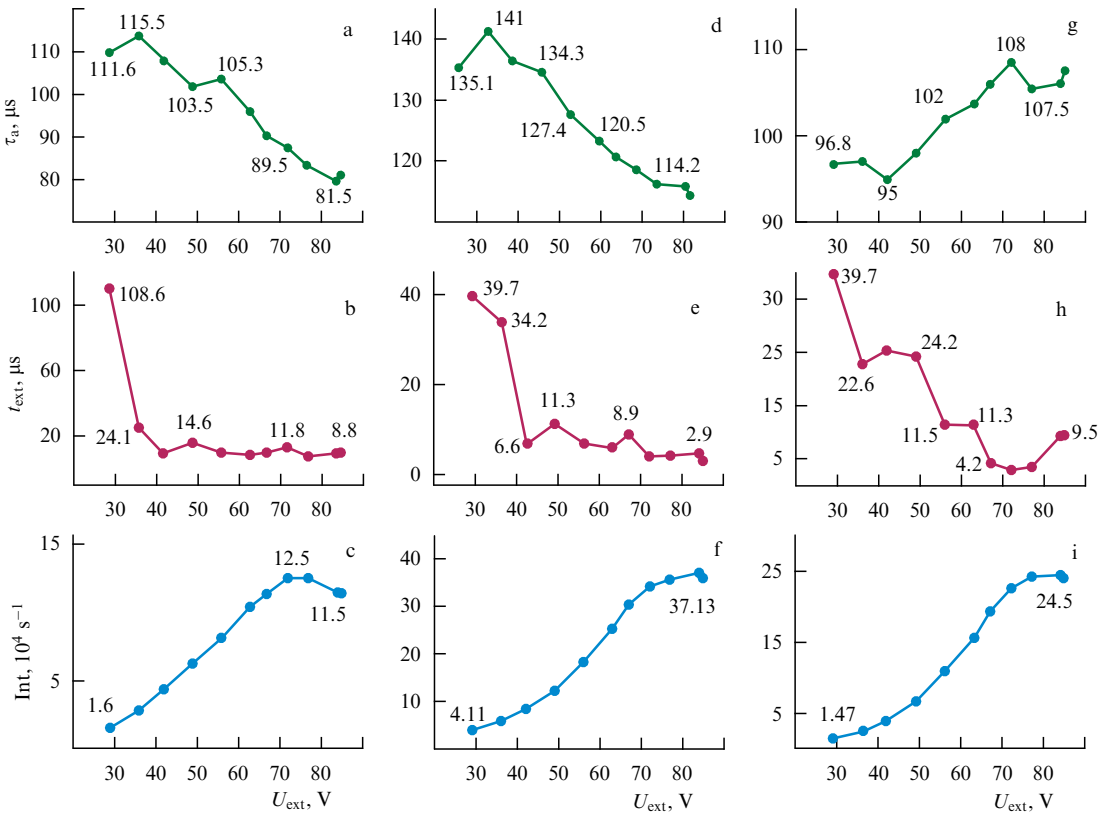

Figure 10. Lifetime (a, d, g), time of ion extraction from ionization chamber (b, e, h), and intensity (c, f, i) of SF_6 molecular negative ions depending on extraction voltage U_{ext}. Measurements with the use of a standard extractor electrode (a–c) and a modified electrode with an interwall distance of 5 mm and a 0.3×10 mm^2 slot for sample inflow (d–f); measurements (g–i) were made with the use of an 18/8 steel extractor electrode described in Ref. [87].

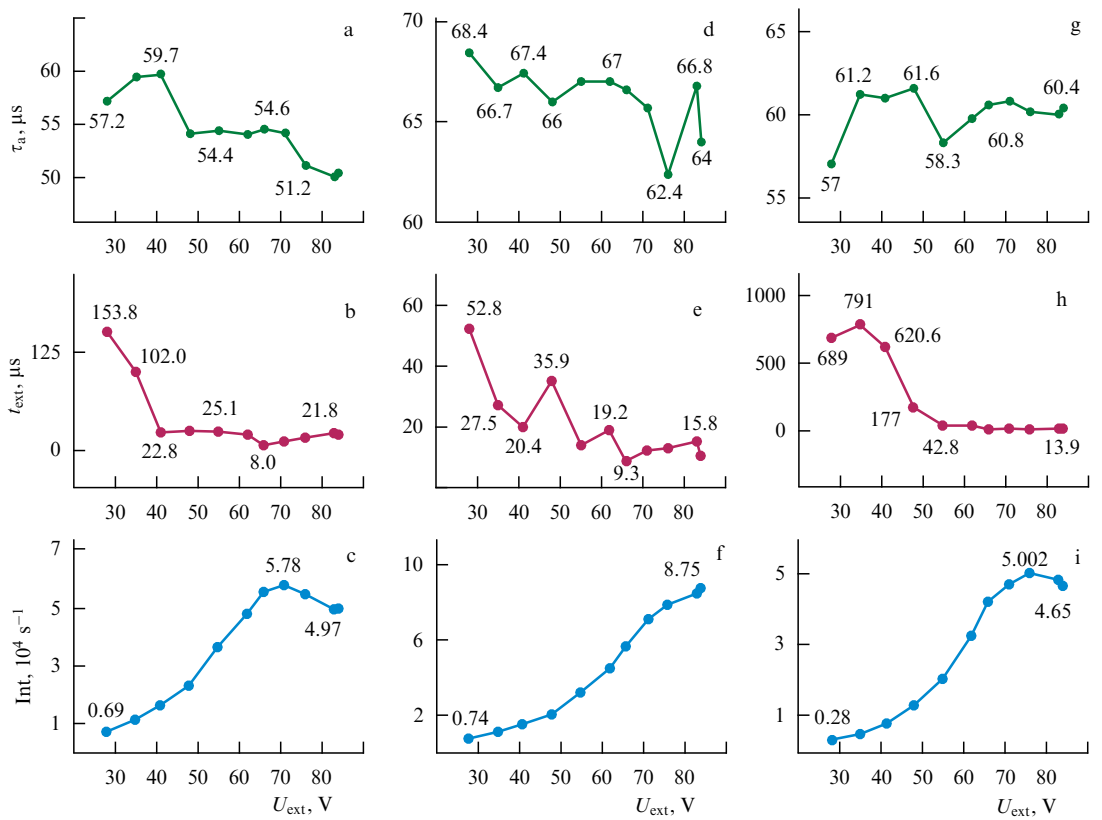

Figure 11. Lifetime (a, d, g), time of ion extraction from ionization chamber (b, e, h), and intensity (c, f, i) of NB molecular negative ions depending on extractor voltage U_{ext}. Measurements (a–c) were made with an 18/8 steel extractor electrode; measurements (d–f) with the use of the same electrode but at a different time, and measurements (g–i) with a modernized split electrode having a 1.6-mm slot as described in Ref. [87].

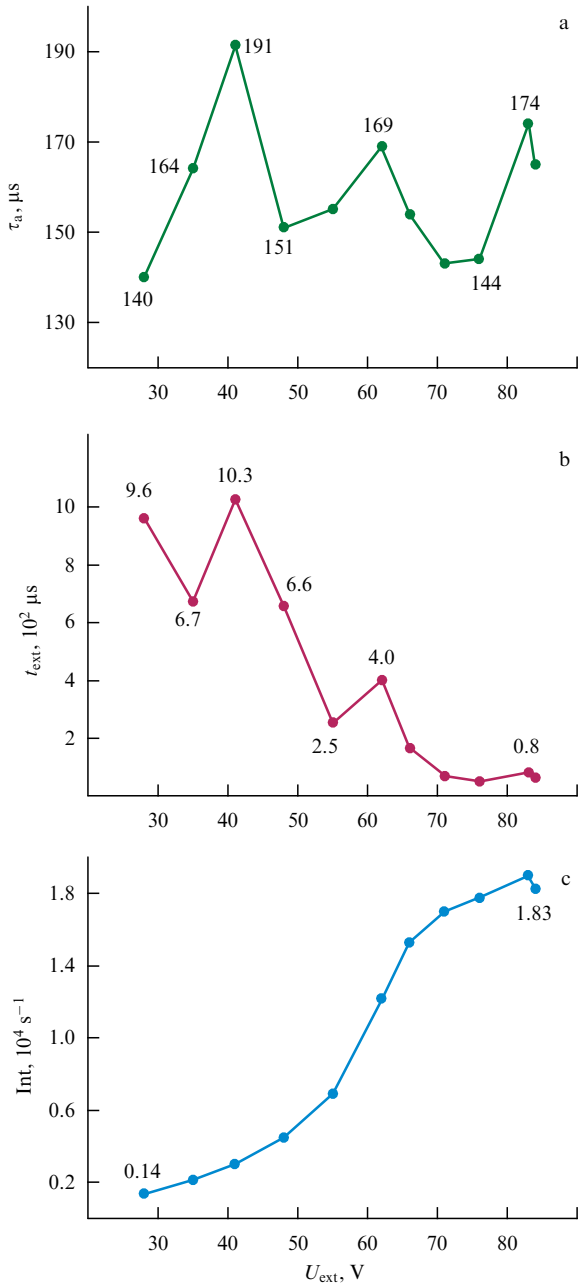

Figure 12. Lifetime (a), time of ion extraction from ionization chamber (b), and intensity (c) of DQ molecular negative ions depending on voltage U_{ext}.

measures to prevent this effect. Specifically, they applied a potential to the walls of the drift chamber to correct the disbalance between the buffer gas flow and clusters near the outlet opening.

The ion adsorption dynamics on the IC walls used in the present study can be described as follows. The entire first part of the negative molecular ions formed in the vacuum chamber upon electron beam unblocking as transient ones with respect to electron autodetachment ($^{a}M^{-}$) is totally adsorbed on the IC walls, where the ions are inevitably stabilized into 'eternal' ones ($^{\infty}M^{-}$). The ions become 'eternal', because they pass onto a lower vibrational level as a result of adhesion to and oscillatory interaction with the surface, which makes impossible electron autodetachment after their desorption back into the vacuum. It is these ions that are recorded in t_{ext} measurements after they leave the surface. However, it is shown below that lifetime measurements reveal the formation of a mixture of stable $^{\infty}M^{-}$ ions and 'ordinary' transient $^{a}M^{-}$ ions that avoided adsorption and appeared in the total ion flux by the time of τ_a measurement.

Importantly, part of the surface $^{\infty}M^{-}$ ions 'survive' (avoid neutralization) and finally desorb back into the vacuum. An ion can 'die' (become neutralized) on the surface due to the tunneling of an additional electron into one of the vacant levels in the conduction band on a given surface. However, this is not always the case. For a negative ion to be neutralized on the surface, certain energy conditions above all must be fulfilled, under which the energy of the orbital with an additional electron in the ion coincides with the conduction rather than valence band having all levels occupied; moreover, some time is needed for the electron tunneling to occur. Therefore, in any case some of the adsorbed $^{\infty}M^{-}$ ions have enough time to desorb into the vacuum before they are neutralized on the surface under favorable energy conditions.

After part of the stable $^{\infty}M^{-}$ ions are released from the IC surface back into the vacuum, they are extracted from the chamber and recorded in the total flux, together with transient $^{a}M^{-}$ ions that failed to attach to the surface. Because $\tau_a(^{\infty}M^{-}) = \infty$, their contribution to the total ion flux increases the measured τ_a; therefore, the greater the stable ion fraction in the flux, the higher experimental τ_a. In other words, the measured τ_a depends on the quantitative relationship between ions of either type, i.e., the $k = N(^{\infty}M^{-})/N(^{a}M^{-})$ ratio that, in turn, must depend on a combination of several factors that may vary uncontrollably from one experiment to the other. This inevitably leads to a scatter of measured τ_a values. Specifically, the fraction of $^{\infty}M^{-}$ ions (hence, the value of k) must depend on such characteristics of the adsorption process as probabilities of ion attachment to the surface, its neutralization on the surface, and ion desorption back into the vacuum. The probability of each of these processes is a function of lens potentials, film thickness, inflow intensity, the physicochemical properties of the surface, the surface band structure, the chemical nature of the molecule of interest, the IC surface area, the size of the outlet slot, and other factors that in the aggregate are likely to distort the measured lifetime.

Ion adsorption on the surface of the IC was directly confirmed in one more experiment described in the next section.

5.3 Complete adsorption of all ions formed after unblocking the electron beam

Experiments with SF_6 and DQ reported earlier in papers [82] and [83], respectively, together with the NB experiment described here (see Table 2) do not merely illustrate the very fact of ion surface adsorption and subsequent desorption but also give evidence that all ions formed immediately after electrons enter the IC are initially adsorbed on its surface. The experiment was designed to separately measure times of ion and neutral molecule extraction [$t_{ext}(M^{-})$ and $t_{ext}(M^{0})$, respectively, where M^{0} is a neutral molecule formed as a product of $^{a}M^{-}$ ion decay with autodetachment of the additional electron]. Time of molecule extraction, $t_{ext}(M^{0})$, was measured upon applying voltage to deflecting plates. In this way, the ion component was removed from the total beam passing through the second zero-field region of the tube to the recording system, so that only the neutral component remained in the beam.

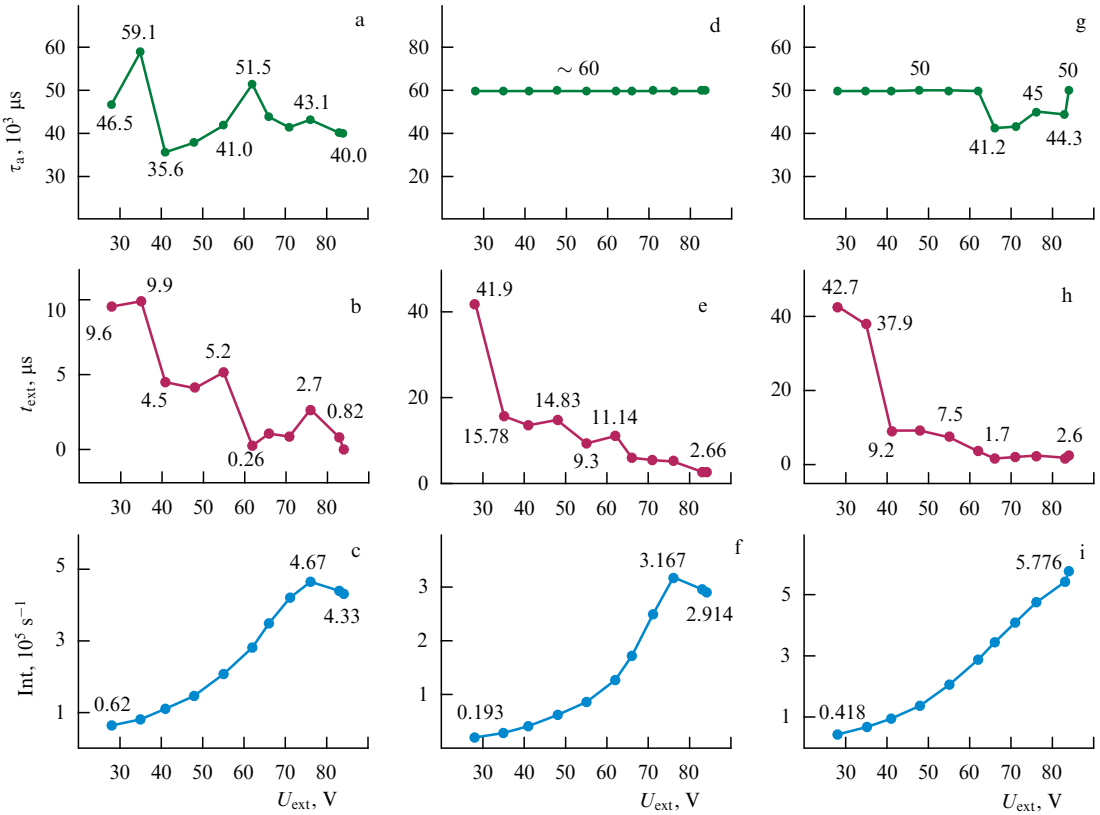

Figure 13. Lifetime (a, d, g), time of ion extraction from ionization chamber (b, e, h), and intensity (c, f, i) of TCNQ molecular negative ions depending on extractor voltage U_{ext}. Measurements (a–c) were made with a standard ion source, measurements (d–f) with the same source, and measurements (g–i) with a modernized split electrode having a 1.6-mm slot as described in Ref. [87].

Table 3. Times $t_{ext}(M^-)$ and $t_{ext}(M^0)$ of negative ion and neutral particle extractions, respectively, from an IC (M^0 is the molecular product of transient negative ion decay resulting from additional electron autodetachment).*

Extraction time, μs	Compound		
	SF_6	DQ	NB
$t_{ext}(M^-)$	5.64	1.38	4.66
$t_{ext}(M^0)$	67.76	61.35	41.9

* Accuracies of $t_{ext}(M^-)$ and $t_{ext}(M^0)$ measurements are ±0.005 and ±0.05 μs, respectively.

From the data collated in Table 3 it follows that in all three compounds considered in this article $t_{ext}(M^0) \gg t_{ext}(M^-)$, the difference amounting to a few tens of microseconds. This means that the ion beam free of the neutral component is the first to leave the IC; in other words, only 'eternal' (stable) $^{\infty}M^-$ ions escape from the chamber. After a relatively long span of time run into a few tens of microseconds they are followed by ordinary transient $^{a}M^-$ ions that avoided adsorption and can lose the additional electron via autodetachment to give rise to neutral M^0 components.

The absence of neutral M^0 molecules in the first ion fraction escaping from the IC suggests that none of the $^{a}M^-$ ions formed immediately after unblocking of the electron beam can leave the IC unless it interacts with the chamber walls, probably because the ions are attracted to the positively charged (with respect to repel electrode) chamber surfaces on their way to the outlet slot, the attractive force being strong enough to deflect their trajectory from the outlet slot toward the surface.

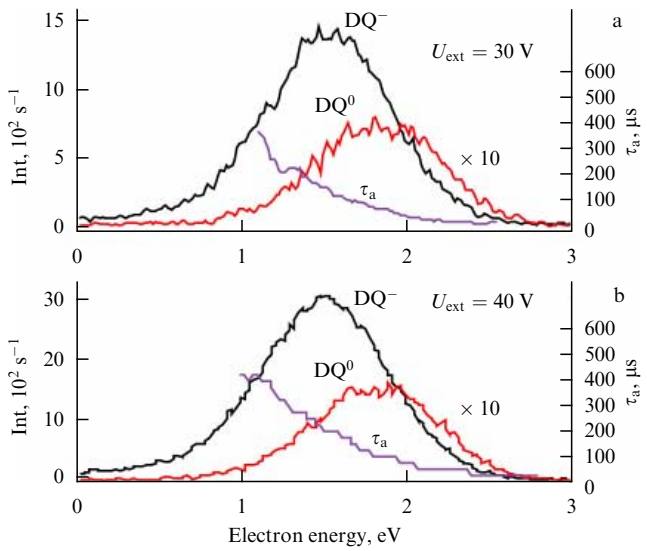

Figure 14. Effective yield curves for DQ^- ions and neutral DQ^0 molecules (ion decay products) and dependences of ion lifetime τ_a on electron energy at U_{ext} = 30 V (a) and U_{ext} = 40 V (b).

Having been adsorbed up to a certain critical number N_1 (the 'first critical number') on the IC walls, the ions eject their first portion into the tube of the analyzer. The instant of time they exit from the IC stands for the time $t_{ext}(M^-)$. As mentioned above, the first portion contains

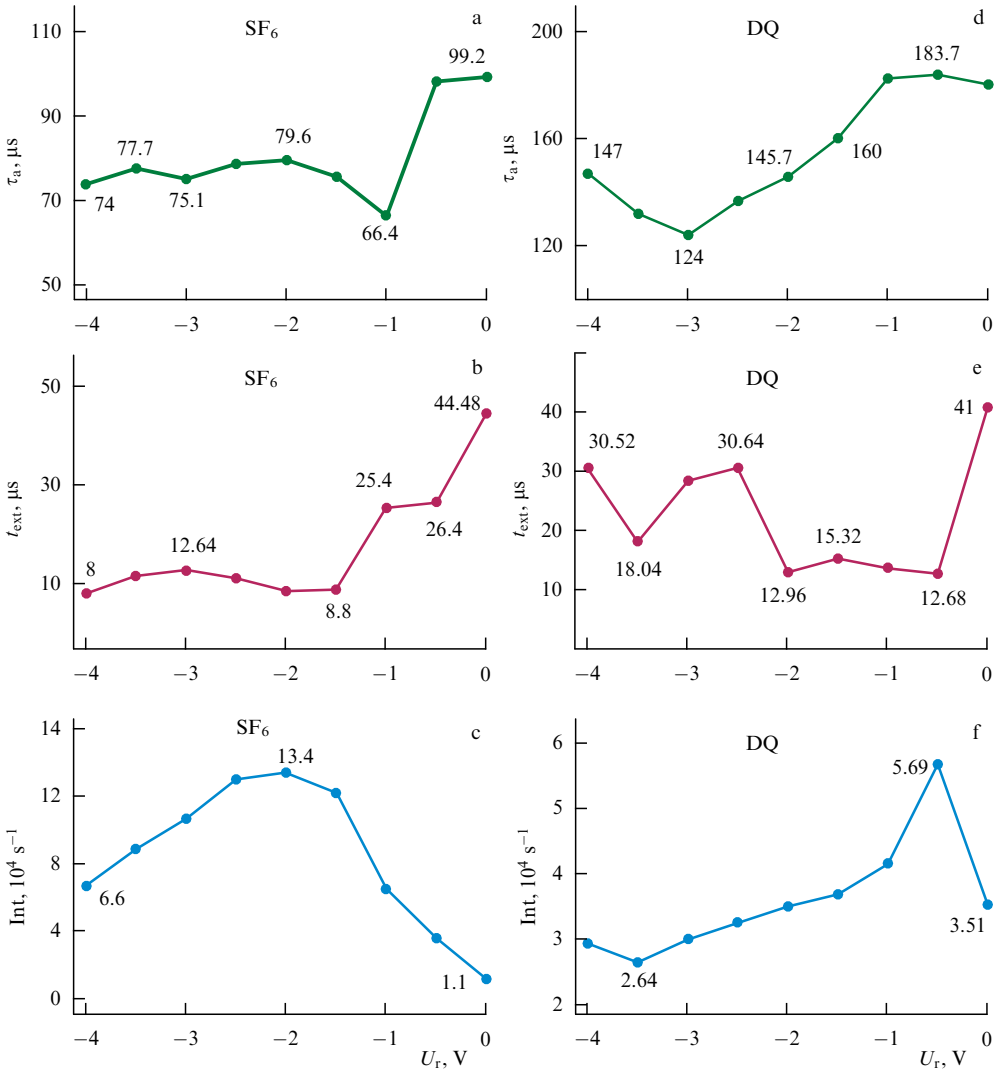

Figure 15. Lifetime (a, d), time of ion extraction from ionization chamber (b, e), and intensity (c, f) of SF_6 and DQ molecular negative ions depending on ejector electrode potential U_r.

stable $^{\infty}M^-$ ions and is free from the neutral component. Thereafter, $^{a}M^-$ ions continue to form in the IC and accumulate on its surface for some time, being unable to escape until the number of surface ions reaches another critical value N_2 (the 'second critical number') and all vacancies on the walls become occupied. Then, a sufficiently thick layer of ions forms on the IC surface and repels newly generated ions from the walls, thereby enabling them to freely fly out of the IC. This flux of outgoing ions contains the neutral component M^0 detected at the instant of time $t_{ext}(M^0)$.

To sum up, ions detached from the IC surface are the first to be registered during t_{ext} measurements. The measured time of their extraction $t_{ext}(M^-)$ is determined by the time of ion accumulation on this surface up to the first critical number N_1, rather than by the time they need to cross the inner IC space.

It should be emphasized once again that adsorbed ions can stay rather long on the IC surface, avoiding there neutralization, because the sufficiently thick film of the study substance on this surface creates a barrier impenetrable for electron tunneling from an ion to the conducting surface; this might substantially reduce the probability of ion neutralization on the surface. Therefore, there can be a certain 'initial' number of ions (N_{in}) deposited on the IC walls during adjustment of the spectrometer by the instants of $t_{ext}(M^-)$ and, possibly, τ_a measurements; then, the time needed to reach the number of ions N_1 may prove shorter than t_{calc}. This leads to satisfying the inequality $t_{ext} < t_{calc}$ that is really observed sometimes. For example, one of the DQ measurements gave $t_{ext}(M^-) = 1.38$ μs (see Table 3), whereas the time of the free escape of this ion from the IC was $t_{calc}(DQ^-) = 6.4$ μs (see Table 2).

Thus, results of analyses in this section and in Section 5.2 give evidence that ions formed in an IC adsorb on its surface. The influence of adsorption on the ion extraction time t_{ext} and measured τ_a is considered in the next section.

5.4 Experimental parameters determining the measured ion lifetime and time of ion extraction from the ionization chamber

It follows from the foregoing (see Section 5.3) that the time t_{ext} of ion extraction from an IC (after unblocking the electron beam) depends on the rate of accumulation (dN/dt) of the critical number N_1 of adsorbed $^{\infty}M^-$ ions being enough to eject their first portion from the IC into the analyzer tube.

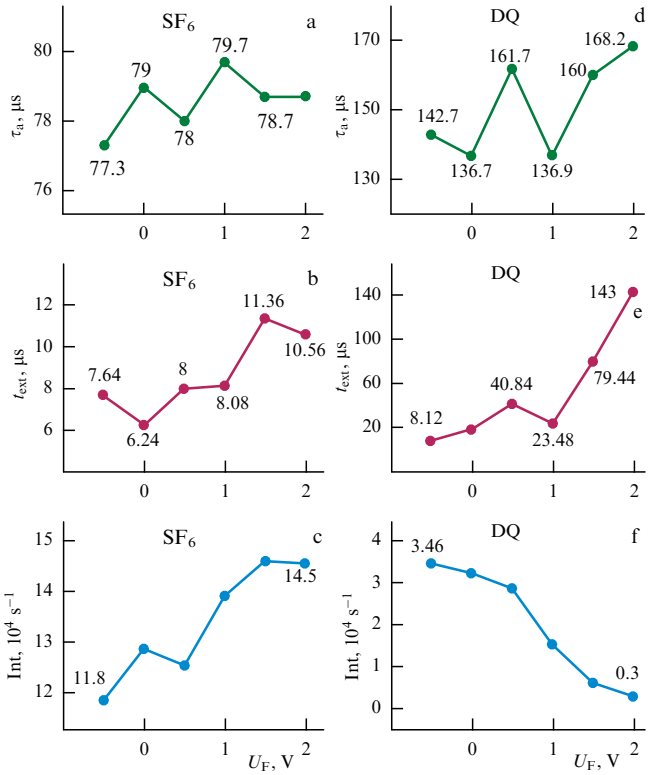

Figure 16. Lifetime (a, d), time of ion extraction from ionization chamber (b, e), and intensity (c, f,) of SF_6 and DQ molecular negative ions depending on first fox potential U_F.

Then, one has

$$N_1 = t_{ext}\,\frac{dN}{dt}\,, \tag{5}$$

and the time needed to accumulate N_1 ions is just t_{ext}.

The measured lifetime τ_a of ${}^aM^-$ ions certainly depends not only on their true duration of existence but also on the ratio of the number of stable ${}^\infty M^-$ ions and transient ${}^aM^-$ ions that reach the recording system during τ_a measurement: $k = N({}^\infty M^-)/N({}^aM^-)$. The value of k is a function of dynamic balance between ions of both types achieved by the instant of measurement. Then, the true lifetime τ can be expressed through the measured lifetime as

$$\tau \sim \frac{\tau_a}{N({}^\infty M^-)/N({}^aM^-)}\,, \tag{6}$$

or

$$\tau \sim \frac{\tau_a}{k}\,. \tag{7}$$

Section 5.5 outlines in general terms those characteristics of the adsorption process that can influence the rate dN/dt and $k = N({}^\infty M^-)/N({}^aM^-)$ ratios.

5.5 Influence of adsorption on ion lifetime and time of ion extraction from the ionization chamber under varied experimental conditions

Results of t_{ext} and τ_a variations under changes of experimental conditions presented in Figs 2–16 are interrelated by virtue of changes in characteristics of the ion adsorption process on the IC surface in response to varying conditions of the experiment. The most noticeable of these characteristics are probabilities of ion adsorption, neutralization on the surface, and desorption back into the vacuum in the case of ion 'survival' on the IC surface. Following are a few examples of the possible influence of these characteristics on t_{ext} and τ_a.

Figures 2b, e, h show that puffing increased amounts of all three substances to be analyzed (SF_6, NB, and DQ) into an IC results in a sharp decrease in t_{ext}. This is quite natural, because the massive inflow of parent materials increases the total number of ions formed in the IC, as is well apparent from their heightened intensity (Figs 2c, f, i). Adsorption increases with increasing inflow, and accumulation of the critical number of ${}^\infty M^-$ ions (N_1) on the surface occurs faster, while t_{ext} decreases. At the same time (see Figs 2c, f, i), the character of τ_a changes is not uniform, being specific for each compound. Lifetime oscillations in SF_6 and DQ are roughly of the same order of magnitude, whereas the lifetime of NB ions decreases. The difference can be attributed to a rise in the total number of ions (not only adsorbed ${}^\infty M^-$ but also transient ${}^aM^-$) formed in the IC. As a result, the $k = N({}^\infty M^-)/N({}^aM^-)$ ratio determining the measured τ_a can simply oscillate, sometimes varying only slightly, as observed in SF_6 and DQ. Sometimes, the relative amount of one of the components increases, e.g., in NB, where the prevalence of ${}^aM^-$ ions results in a decrease in τ_a.

In contrast, experiments with a heated IC revealed a rise in t_{ext} with temperature (Figs 4b, e, h and 5b), attributable to ion neutralization on the surface due to the tunneling of an additional electron to the surface.

As mentioned above in Section 5.2, the possibility of electron tunneling from an ion to the IC surface depends on the energy characteristics of the IC surface band structure (in the present case, 18/8 stainless steel coated with soot for absorption of slow electrons [94]) and ions with energy levels stabilized by the charge induced in the conducting surface [95] and the positive potential applied to the IC.

Neutralization of ions of all the compounds studied in the present work is possible. It occurs with a greater or lesser probability, depending on the width of the tunneling barrier formed by the molecular layer (film) of the injected substance between the ions and the surface [96]. A rise in IC temperature decreases the film thickness and narrows the barrier; as a result, the probability of electron tunneling increases and ion neutralization proceeds more efficient.

Neutralization of newly formed and adsorbed ions at elevated temperatures is manifested as a lowered intensity of the recorded ion flux (Figs 4g, h, i and 5c). That intensity lowering was primarily due to neutralization of adsorbed ions was confirmed in experiments with Cl^- ions from trichlorethylene (C_2HCl_3), in which such a temperature-dependent decrease in intensity does not occur [82]. A Cl^- ion cannot release the additional electron into the surface, since its energy characteristics do not match the band structure of the IC surface, which, in principle, rules out the possibility of its neutralization on the IC surface.

It is worthwhile to note that similar results concerning the role of the intermediate layer (n-hexane and Kr) and the band structure in negative ion neutralization on the Pt surface were also reported earlier by other authors [97].

The effect of the ion neutralization factor on t_{ext} and τ_a can be described as follows. Ion extraction time t_{ext} must increase with increasing probability of ion neutralization, because more time is needed for the critical number of ions N_1 to accumulate under conditions of enhanced ion death on the surface. At the same time, τ_a must decrease, since the death of

$^{\infty}M^-$ ions shifts the $^{\infty}M^-$-to-$^{a}M^-$ ratio in favor of the latter. Such changes (increase in t_{ext} and reduction of τ_a) were indeed documented for SF_6, NB, and DQ in association with a rise in IC temperature (see Fig. 4).

At the same time, Fig. 5 clearly shows that TCNQ deviates from this pattern. The differences between TCNQ, on the one hand, and SF_6, NB, DQ, on the other hand, are due to more intense ion desorption from the IC surface, corresponding to well-known stronger desorption of the parent compound during conventional temperature annealing of the chamber. The conclusion about the greater role of ion desorption in the case of TCNQ is based on the fact that an elevated temperature does not cause a reduction in $TCNQ^-$ ion intensity (due to a weaker ion neutralization). The enhanced probability of desorption can, in turn, be a consequence of the formation of a thick film of TCNQ molecules on the IC walls that resists its thinning despite temperature growing. A similar phenomenon is known to take place in thick films of other materials even at high temperatures [98].

Increased ion desorption similarly affects t_{ext} and τ_a: both increase, because the loss of adsorbed $^{\infty}M^-$ ions from the surface results in slower accumulation of their critical number N_1, whereas a greater number of the same $^{\infty}M^-$ ions entering the total ion flux shifts the $^{\infty}M^-$-to-$^{a}M^-$ ratio in favor of the former. In other words, temperature-induced ion desorption causes t_{ext} and τ_a to change in synchrony. In addition, this effect can combine with that of neutralization. A combination of these effects actually takes place in SF_6, NB, and DQ. It follows from Fig. 4 that the general tendency toward a t_{ext} increase and a τ_a decrease in these compounds is superimposed by one more (weaker) dependence similar to the higher harmonic (see above) responsible for synchronous changes in t_{ext} and τ_a. At the same time, in TCNQ, such a 'harmonic' is a major feature (Figs 5a, b) underlying the direct correlation between t_{ext} and τ_a, which suggests the predominant influence of ion desorption on the measured t_{ext} and τ_a values.

The above analysis gives evidence that the 'true' temperature dependence of τ_a arising from the thermal population of vibrational levels in parent molecules can be deeply concealed by adsorption effects, as shown for SF_6 and DQ in Refs [82, 83] and for NB in the present work (see Fig. 4).

In fact, a rise in IC temperature from 333 to 473 K in the case of NB results in a roughly 16-fold reduction in ion beam intensity (from $\sim 2.4 \times 10^4$ to 1.5×10^3 pulses/s). Such a sharp decrease in ion intensity cannot be accounted for by the 'true' temperature dependence alone, even on the assumption that τ_a of vibrationally excited molecular ions is so small that they are practically unable to reach the recording system; the number of molecules at the ground vibrational level cannot decrease 16-fold upon temperature elevation from 333 to 473 K. Indeed, the ratio of the number of molecules at the first excited vibrational level (N_1) to that at the ground one (N_0) is expressed in accordance with the Boltzmann distribution as

$$\frac{N_1}{N_0} = \exp\left(-\frac{\Delta E}{k_B T}\right), \tag{8}$$

where ΔE is the energy of the first excited vibrational level in cm^{-1}, $k_B = 8.6112 \times 10^{-5}$ eV K^{-1} is the Boltzmann constant, and T is the IC temperature in kelvins.

For $C_6H_5NO_2$, $\Delta E = 51$ cm^{-1} (0.0063232 eV) [99]. It follows from Eqn (8) that $(N_1/N_0)' = 0.08021093$ at $T_1 = 333$ K, and $(N_1/N_0)'' = 0.8562071$ at $T_2 = 473$ K. Since the total number of molecules remains unaltered, i.e., $(N_1 + N_0)' = (N_1 + N_0)''$, then $N_0'/N_0'' \approx 1.03$. In other words, a rise in IC temperature from 333 to 473 K causes a 1.03-fold reduction in the population of the zero vibrational level. Therefore, the intensity of $C_6H_5NO_2^-$ ions in the case of 'true' temperature dependence can decrease by 1.03 times at best, but not by 16 times, which means that such a dramatic drop in intensity is due to a decrease in the relative number of $^{\infty}M^-$ ions in the total beam as a result of $^{\infty}M^-$ neutralization on the IC surface, rather than to a decreased population of the zero vibrational level at an elevated temperature.

We also studied variations of t_{ext} and τ_a under the effect of helium injection into the IC together with a substance to be analyzed (see Figs 7 and 8). The amount of helium being introduced gradually increased during the experiment. The results were similar to those obtained in the studies with increasing temperature. The similarity with temperature dependences was most pronounced in experiments with SF_6 (see Fig. 7), DQ and especially TCNQ (see Fig. 8). Enlarged amounts of helium introduced into the IC caused t_{ext} to increase and τ_a to decrease exactly in the same way as temperature elevation did. The decrease in τ_a (TCNQ) amounted to two orders of magnitude in association with a fivefold reduction in measured $TCNQ^-$ ion intensity, allowing the conclusion that effects of either factor have a common cause, namely, the thinning of the films formed by the two compounds on the IC walls, which promotes ion neutralization enhancement. The only difference between effects of the enlarged amount of helium and elevated IC temperature is that film thinning in the former case is due to the washout of the substance of interest by helium. This phenomenon is widely known and used in gas flow cleaning of contaminated surfaces [100].

In a similar experiment with helium injection, NB molecular ions exhibited a somewhat different behavior. Specifically, the introduction of enlarged amounts of helium increased τ_a and decreased t_{ext}, as in the TCNQ experiment at elevated temperatures. In the case of NB, τ_a on the whole increased but insignificantly, while a change in t_{ext}, if any, was almost unnoticeable (Figs 7d, e), as fully corroborated by an appreciable direct correlation between t_{ext} and τ_a (the 'high harmonic') that is a characteristic feature of the desorption effect (see above). In the case of NB, this effect prevails in the influence on t_{ext} and τ_a measurements. It is equally well apparent in SF_6 (Figs 7a, b). Although it does not completely suppress the neutralization effect responsible for the general increase in t_{ext} with a simultaneous τ_a decrease, nonetheless it is clearly manifested in the form of the aforementioned 'higher harmonic' superimposed on the main trend of t_{ext} and τ_a plots.

Results of SF_6, NB, DQ, and TCNQ experiments with an increased extractor electrode potential (see Figs 10–13) are equally well consistent with the ion adsorption concept. A rise in U_{ext} causes ion intensity to increase and t_{ext} to decrease, because fewer adsorbed $^{\infty}M^-$ ions are needed to eject their first portion from the IC at higher U_{ext}. As a result, the critical number N_1 (hence t_{ext}) decreases. The intensity grows because fewer newly formed ions are adsorbed and neutralized as U_{ext} increases. Lifetime (τ_a) sometimes decreases, e.g., in SF_6 (Figs 10a, d) and in NB (Figs 11a, d), evidently due to a smaller fraction of $^{\infty}M^-$ ions in the general ion flux. In other cases, τ_a either increases, e.g., in SF_6 (Fig. 10g), or oscillates

near a constant value, as in NB (Fig. 11g), DQ (Fig. 12a), and TCNQ (Figs 13a, d, g).

The cause of such an ambiguous dependence of τ_a on U_{ext} lies in the fact that extractor voltage cannot only decrease adsorption and thereby enlarge the $^aM^-$ ion fraction in the total flux, it can also foster ion desorption and increase the $^\infty M^-$ ion fraction. It results in arbitrary variations of the $^\infty M^-/^aM^-$ ratio responsible for a variety of τ_a changes. To recall, some measurements for one and the same compound were made using extractor electrodes of various designs.

It might be concluded that two factors exert the dominant influence on t_{ext} and τ_a with enhancing U_{ext}, viz. the probability of ion adsorption on the surface and the probability of ion desorption. The second factor clearly manifests itself in SF_6 (Fig. 10d, e), DQ (Fig. 12a, b), and TCNQ (Fig. 13g, h), as usual in the form of the 'higher harmonic' on t_{ext} and τ_a plots of the direct relationship between these quantities.

Changes to t_{ext} and τ_a also occur upon varying two other ion source potentials, viz. U_r at the repel electrode (see Fig. 15) and U_F at the first fox (see Fig. 16). Variation of U_r in SF_6 and U_F in DQ reveals a direct correlation between t_{ext} and τ_a. Moreover, there is a reverse correlation apparent in SF_6 upon a change in U_F. At the same time, no relationship between t_{ext} and τ_a associated with U_r changes is observed in DQ. In other words, there is no obvious interdependence between t_{ext} and τ_a, probably due to the effect of a complex combination of fields, potentials, and charges in the IC. This is yet more evidence of the absence of correlation between t_{ext} and τ_a and, therefore, of the large role of the ion adsorption process in the experiment.

6. Influence of surface adsorption on measurement results

The data obtained can be briefly summarized as follows. It was demonstrated in experiment that the time of negative ion extraction from the ionization chamber of the static sector magnetic mass spectrometer is frequently much longer than the free-flight time of ion escape from the IC. It is therefore concluded that part of the transient negative ions formed in autodetachment states adsorb on its surface before they leave the chamber. The adsorbed ions are then stabilized on the surface. Some of them undergo neutralization and cannot participate in further processes. However, a certain part of the adsorbed ions desorb back into a vacuum, join the total ion flux, and thereby distort the measured lifetime, overestimating its duration, because the stabilized surface ions returning to the vacuum are unable to liberate the additional electron and therefore have 'an infinitely long lifetime' which creates the semblance of an overall increase in its duration.

Thus, surface adsorption influences both measured quantities, namely, the ion lifetime with respect to electron autodetachment and the time of ion extraction from the ionization chamber. Adsorption characteristics (time of ion retention on the surface, numbers of absorbed and desorbed ions) depend on the experimental conditions. For this reason, the measured ion lifetime and time of their extraction from the IC change significantly upon varying these conditions. The two quantities do not correlate, at variance with the universally accepted multiexponential decay concept. It is also shown that the abnormally sharp decrease in the ion lifetime with rising temperature is due to a reduced number of stable ions in the total ion flux resulting from the enhanced effectiveness of their surface neutralization at elevated temperatures rather than to changes in the population of vibrational levels in the parent molecules.

It is worthy of note that the conclusion about negative ion adsorption on the chamber walls is based on the results of measurements with the aid of a static sector magnetic mass spectrometer. Such adsorption may prove indistinctive for time-of-flight mass spectrometers. Nevertheless, there is every reason to widely employ the instrumentation used in the present study, bearing in mind the advantages it provides, and first of all its high sensitivity, which is at least an order of magnitude higher than that of time-of-flight mass spectrometers. The advantages of the static sector magnetic mass spectrometer became especially apparent when the two techniques were employed to study the same substances. One of them is parabenzoquinone ($O{=}C_6H_4{=}O$), in which 10 types of the formerly unknown fragment negative ions were recorded [28]. Another example is Cl-ethylenes for which the curves of effective NI yield in a high-energy region were obtained for the first time, which made it possible to elucidate the respective electron capture mechanisms [24].

7. Conclusion

This article presents an original experimental technique intended to study long-lived autodetachment states of negative ions whose lifetimes τ_a with respect to autodetachment of the additional electron amount to several microseconds or more, i.e., by 8–9 orders of magnitude greater than those of 'ordinary' autodetachment states formed in the process of slow-electron resonance attachment to molecules [4]. Such long-living negative ions are of great interest by virtue of their fundamental role in radiation chemistry, aeronomy, electron impact spectroscopy, biophysics, and many other fields. It accounts for the close attention that has been given to the mechanisms of their formation and decay in many laboratories in recent decades.

Quantity τ_a is the most important characteristic of long-lived ions. Its experimental and theoretical evaluation provides information about the structure and stereoisomerism of parent molecules. Moreover, these estimates can be applied for the qualitative analysis of extrapure substances and for determining the type of resonance being observed.

For many years, researchers have encountered the problem of scatter of experimentally measured τ_a values. The present study done with the use of the aforementioned mass spectrometer showed that one of the causes for the scatter is adsorption of a part of the ions formed in an ionization chamber on its surface responsible for their stabilization into 'eternal' particles, followed by their partial desorption back into a vacuum, where they join the total ion flux. These ions, together with 'ordinary' transient ones, reach the time recording system and distort the measured τ_a values, overestimating them due to their 'infinitely long' lifetime. The error of τ_a measurements can be of any magnitude, because it depends on the number of adsorbed and desorbed ions, which, in turn, varies with experimental conditions, frequently leading to an uncontrollable scatter. It should be emphasized that ion adsorption on the ionization chamber walls is a usual well-known phenomenon. A new finding reported in the present article is that only part of the adsorbed ions undergo neutralization on the surface; many of them can detach from it to return into the vacuum and thereby negatively affect experimental results.

The discovery of ion adsorption on the surface of the ionization chamber and their subsequent desorption toward the recording system resulting in the distortion of the measured lifetime opens up some new prospects for research into autodetachment states of long-lived negative ions. First, taking account of this phenomenon allows understanding certain thus far obscure peculiarities of mass spectrometry-based experiments. Second, it may help to improve the accuracy of τ_a measurements by means of choosing more adequate experimental conditions and reducing to a minimum the negative effect of desorbed ions, e.g., the puffing of an inert gas into the ionization chamber to promote surface ion neutralization due to washout of the substance of interest from the film and thereby to decrease the number of desorbed ions. Equally beneficial may be shifting the lens potentials in the ion source toward negative values, as described earlier in Ref. [93]. In this way, ion adsorption itself can be reduced to a minimum. Results of the present study appear to be of theoretical interest as well, providing deeper insight into the thermal population of vibrational levels of a parent molecule producing a negative ion and its influence on the lifetime of autodetachment states.

Acknowledgments

The authors gratefully acknowledge P V Shchukin and R V Khatymov, the staff members of the Institute of Molecular and Crystal Physics, Ufa Scientific Center of RAS, for the detailed discussion of our work, which provided a more complete understanding of its results. We also wish to thank the reviewer for his deep and very accurate observations contributing to bringing the work, in our opinion, to a higher qualitative level.

This work was financially supported by the Russian Foundation for Basic Research (grant 11-02-97071-r Povolzh'e a) and by the Federal Agency of Scientific Organizations (project No. 0248-2014-005:14.5).

References

1. Massey H S W *Negative Ions* (Cambridge: Cambridge Univ. Press, 1976)
2. Smirnov B M *Negative Ions* (New York: McGraw-Hill, 1982)
3. Schulz G J *Rev. Mod. Phys.* **45** 423 (1973)
4. Illenberger E, Smirnov B M *Phys. Usp.* **41** 651 (1998); *Usp. Fiz. Nauk* **168** 731 (1998)
5. Khvostenko V I, Tolstikov G A *Russ. Chem. Rev.* **45** 127 (1976); *Usp. Khim.* **45** 251 (1976)
6. Simons J *Annu. Rev. Phys. Chem.* **62** 107 (2011)
7. Christophorou L G, Grant M W, McCorkle D L *Adv. Chem. Phys.* **36** 413 (1977)
8. Christophorou L G, in *Advances in Electronics and Electron Physics* (Ed. L Marton) (New York: Academic Press, 1978) p. 55
9. Compton R N, Cooper C D *J. Chem. Phys.* **59** 4140 (1973)
10. Feshbach H *Ann. Physics* **5** 357 (1958)
11. Fano U *Phys. Rev.* **124** 1866 (1961)
12. Feshbach H *Ann. Physics* **19** 287 (1962)
13. Demkov Yu N *Sov. Phys. JETP* **22** 615 (1966); *Zh. Eksp. Teor. Fiz.* **49** 885 (1965)
14. Demkov Yu N *Phys. Lett.* **15** 235 (1965)
15. Taylor H S, Nazaroff G V, Golebiewski A *J. Chem. Phys.* **45** 2872 (1966)
16. O'Malley T F *Phys. Rev.* **150** 14 (1966)
17. Bardsley J N, Mandl F *Rep. Prog. Phys.* **31** 471 (1968)
18. Herzenberg A *J. Chem. Phys.* **51** 4942 (1969)
19. Taylor H S, Thomas L D *Phys. Rev. Lett.* **28** 1091 (1972)
20. Drukarev G F *Collisions of Electrons with Atoms and Molecules* (New York: Plenum Press, 1987); Translated from Russian: *Stolknoveniya Elektronov s Atomami i Molekulami* (Moscow: Nauka, 1978)
21. Illenberger E, Smirnov B M *High Temp.* **38** 829 (2000); *Teplofiz. Vys. Temp.* **38** 862 (2000)
22. Dressler R, Allan M, Tronc M *J. Phys. B* **20** 393 (1987)
23. Khvostenko V I, Vorob'ev A S, Khvostenko O G *J. Phys. B* **23** 1975 (1990)
24. Khvostenko O G et al. *J. Electron Spectrosc. Relat. Phenom.* **199** 1 (2015)
25. Sweetman D R *Proc. Phys. Soc. London* **76** 998 (1960)
26. Allan M *Chem. Phys.* **84** 311 (1984)
27. Khvostenko O G, Tuimedov G M *Rapid Commun. Mass Spectrom.* **20** 3699 (2006)
28. Khvostenko O G, Tuimedov G M, Dzhemilev U M *Dokl. Phys. Chem.* **414** 162 (2007); *Dokl. Ross. Akad. Nauk* **414** 784 (2007)
29. Khvostenko O G et. al. *Int. J. Mass Spectrom.* **273** 69 (2008)
30. Khvostenko O G, Lukin V G, Tseplin E E *Rapid Commun. Mass Spectrom.* **26** 2535 (2012)
31. Vardya M S, Krishna S K S *Chem. Phys. Lett.* **73** 626 (1980)
32. Sarre P J *J. Chim. Phys. Phys. Chim. Biol.* **77** 769 (1980)
33. Pikaev A K *Sovremennaya Radiatsionnaya Khimiya: Osnovnye Polozheniya. Eksperimental'naya Tekhnika i Metodika* (Modern Radiation Chemistry: Fundamentals, Experimental Techniques and Methods) (Moscow: Nauka, 1985)
34. Kaplan I G *Khim. Vys. Energ.* **17** 210 (1983)
35. Hickam W M, Fox R E *J. Chem. Phys.* **25** 642 (1956)
36. Edelson D, Grifiths J E, McAffe R B *J. Chem. Phys.* **37** 917 (1962)
37. Khvostenko V I *Mass-spektrometriya Otritsatel'nykh Ionov v Organicheskoi Khimii* (Mass-Spectrometry of Negative Ions in Organic Chemistry) (Moscow: Nauka, 1981)
38. Liu Y, Suess L, Dunning F B *J. Chem. Phys.* **122** 214313 (2005)
39. Pajput J, Lammich L, Andersen L H *Phys. Rev. Lett.* **100** 153001 (2008)
40. Menk S et al. *Phys. Rev. A* **89** 022502 (2014)
41. Henis J M S, Mabie C A *J. Chem. Phys.* **53** 2999 (1970)
42. Odom P W, Smith D L, Futrell J H *Chem. Phys. Lett.* **24** 227 (1974)
43. Odom P W, Smith D L, Futrell J H *J. Phys. B* **8** 1349 (1975)
44. Compton R N et al. *J. Chem. Phys.* **45** 4634 (1966)
45. Naff W T, Compton R N, Cooper C D *J. Chem. Phys.* **54** 212 (1971)
46. Harland P W, Thynne J C J *J. Phys. Chem.* **75** 3517 (1971)
47. Khvostenko V I et al. *Izv. Akad. Nauk SSSR Ser. Khim.* **3** 680 (1973)
48. Vorob'ev A S *Tech. Phys.* **54** 1255 (2009); *Zh. Tekh. Fiz.* **79** (9) 11 (2009)
49. Naff W T, Cooper C D, Compton R N *J. Chem. Phys.* **49** 2784 (1968)
50. Lukin V G, Vorob'ev A S, Lomakin G S *Instrum. Exp. Tech.* **52** 560 (2009); *Prib. Tekh. Eksp.* (4) 121 (2009)
51. Thyne J C J, Harland P W *Int. J. Mass Spectrom. Ion Phys.* **11** 137 (1973)
52. Christophorou L G *Atomic and Molecular Radiation Physics* 2nd ed. (London: Wiley-Interscience, 1978)
53. Compton R N, Bouby L *Comp. Rend. Acad. Sci.* **264** 1153 (1967)
54. Hadjiantoniou A, Christophorou L G, Carter J G *J. Chem. Soc. Faraday Trans. 2* **69** 1704 (1973)
55. Cooper C D, Compton R N *J. Chem. Phys.* **59** 3550 (1973)
56. Christophorou L G, Hadjiantoniou A, Carter J G *J. Chem. Soc. Faraday Trans. 2* **69** 1713 (1973)
57. Hadjiantoniou A, Christophorou L G, Carter J G *J. Chem. Soc. Faraday Trans. 2* **69** 1691 (1973)
58. Stockdale J A, Compton R N, Schwinler H C *J. Chem. Phys.* **53** 1502 (1970)
59. Christophorou L G *Atomic and Molecular Radiation Physics* (London: Wiley-Interscience, 1971)
60. Harland P W, Thyne J C J *Inorgan. Nucl. Chem. Lett.* **7** 29 (1971)
61. Kukhta A V et al. *Int. J. Mass Spectrom.* **230** 41 (2003)
62. Khatymov R V, Tuktarov R F, Muftakhov M V *JETP Lett.* **93** 437 (2011); *Pis'ma Zh. Eksp. Teor. Fiz.* **93** 482 (2011)
63. Pshenichnyuk S A et al. *Russ. J. Phys. Chem. B* **4** 1014 (2010); *Khim. Fiz.* **29** (11) 82 (2010)
64. Christophorou L G, Carter J G, Christodoulides A A *Chem. Phys. Lett.* **3** 237 (1969)
65. Collins P M et al. *Chem. Phys. Lett.* **4** 646 (1970)

66. Cooper C D, Naff W T, Compton R N *J. Chem. Phys.* **63** 2752 (1975)
67. Khvostenko O G, Lukin V G, Tseplin E E *Rapid Comm. Mass Spectrom.* **26** 2535 (2012)
68. Begun G M, Compton R N *J. Chem. Phys.* **58** 2271 (1973)
69. Khvostenko V I et al. *Bull. Acad. Sci. USSR Chem. Ser.* **26** 655 (1977); *Izv. Akad. Nauk SSSR Ser. Khim.* (3) 717 (1977)
70. Compton R N, Cooper C D *J. Chem. Phys.* **66** 4325 (1977)
71. Khvostenko O G et al. *Butlerov. Soobshch.* **35** (8) 9 (2013)
72. Mazunov V A et al. *Bull. Acad. Sci. USSR Chem. Sci.* **32** 197 (1983); *Izv. Akad Nauk SSSR Ser. Khim.* (1) 223 (1983)
73. Vasil'ev Y V, Mazunov V A, Nazirov E R *Org. Mass Spectrom.* **26** 739 (1991)
74. Tuktarov R F et al. *JETP Lett.* **90** 515 (2009); *Pis'ma Zh. Eksp. Teor. Fiz.* **90** 564 (2009)
75. Vasil'ev Y V et al. *Fuller. Nanotub. Carbon Nanostruct.* **12** 229 (2004)
76. Foster M S, Beanchamp J L *Chem. Phys. Lett.* **31** 482 (1975)
77. Le Garrec J-L, Steinhurst D A, Smith M A *J. Chem. Phys.* **114** 8831 (2001)
78. Suess L, Parthasarathy R, Dunning F B *J. Chem. Phys.* **117** 11222 (2002)
79. Cannon M et al. *J. Phys. Chem.* **127** 064314 (2007)
80. Klots C E *J. Phys. Chem.* **46** 1197 (1967)
81. Lukin V G, Lomakin G S *Instrum. Exp. Tech.* **53** 401 (2010); *Prib. Tekh. Eksp.* (3) 88 (2010)
82. Lukin V G, Khvostenko O G, Tuimedov G M *Int. J. Mass Spectrom.* **399** 17 (2016)
83. Lukin V G, Khvostenko O G, Tuimedov G M *Tech. Phys. Lett.* **42** 215 (2016); *Pis'ma Zh. Tekh. Fiz.* **42** (4) 96 (2016)
84. Barzilovich P P et al. *Prib. Sist. Upravl.* (1) 24 (1971)
85. Savin O R *Prib. Sist. Upravl.* (10) 13 (1983)
86. Khvostenko V I et al. *Khim. Fiz.* (7) 915 (1982)
87. Lukin V G, Tuimedov G M *Instrum. Exp. Tech.* **56** 565 (2013); *Prib. Tekh. Eksp.* (5) 77 (2013)
88. Ustroistvo Interfeisnoe (Tekhnicheskoe Opisanie i Instruktsiya po Ekspluatatsii (The Interface Device (Technical Description and Operational Manual)) (Chernogolovka: NTO AN SSSR, 1989)
89. Trokhov S E et al. *Prib. Tekh. Eksp.* (3) 255 (1975)
90. Lukin V G, Fal'ko V S, Vyazovkin D E *Avtometriya* (1) 111 (1992)
91. Rukovodstvo po Ekspluatatsii Tsifrovogo Ostsillografa Serii GDS-820S (GDS-820S Digital Oscillograph. Operational Manual) (Moscow, 2007)
92. Granovskii V L *Elektricheskii Tok v Gaze* (*Ustanovivshiisya Tok*) (Electrical Current in a Gas: Steady Current) (Moscow: Nauka, 1971)
93. Kashtanov P V, Smirnov B M, Hippler R *Phys. Usp.* **50** 455 (2007); *Usp. Fiz. Nauk* **177** 499 (2007)
94. Roberts T D, Burch B S *Rev. Sci. Instrum.* **35** 1067 (1964); Translated into Russian: *Prib. Nauch. Issled.* (8) 140 (1964)
95. Sanche L *J. Phys. B* **23** 1597 (1990)
96. Datta S et al. *Phys. Rev. Lett.* **79** 2530 (1997)
97. Waddill G D, Kesmodel L L *Phys. Rev. B* **32** 2107 (1985)
98. Dushman S *Scientific Foundations of Vacuum Technique* (New York: Wiley, 1962); Translated into Russian: *Nauchnye Osnovy Vakuumnoi Tekhniki* (Moscow: Mir, 1964)
99. Clarkson J, Smith W E *J. Mol. Stuct.* **655** 413 (2003)
100. *Physik und Technik von Sorptions- und Desorptions-vorgängen bei niederen Drücken* (Esch: R.A. Lang, 1963); Translated into Russian: *Sorbtsionnye Protsessy v Vakuume* (Moscow: Atomizdat, 1966) p. 87